UNIVERSITÀ DEGLI STUDI DI PALERMO

Dottorato di Ricerca in Biomedicina e Neuroscienze
Dipartimento di Biomedicina e Neuroscienze Cliniche (BioNeC)
SSD BIO/09

CHARACTERIZATION OF THE SYNAPTIC PROTEOME IN NON-DEMENTED SUBJECTS WITH ALZHEIMER'S NEUROPATHOLOGY

LA CANDIDATA
Dott. Olga Zolochevska

LA COORDINATRICE
Chiar.ma Prof.Felicia Farina

IL CO-TUTOR
Chiar.mo Prof. Giulio Taglialatela

TUTOR
Chiar.ma Prof. Flavia Mulé

CICLO XXX
ANNO 2016/2017

TABLE OF CONTENTS

DISCLOSURE

Research reported in this thesis was supported by the National Institute of Environmental Health Sciences of the National Institutes of Health under award number T32ES007254, National Institute On Aging of the National Institutes of Health under award number F31AG057217.

Publications that resulted from this work:

1. **Zolochevska, O** and Taglialatela, G. Non-demented individuals with Alzheimer's disease neuropathology: resistance to cognitive decline may reveal new treatment strategies. *Current Pharmaceutical Design*. 2016 May 18. [Epub ahead of print]
2. **Zolochevska, O**, Bjorklund, N, Woltjer, R, Wiktorowicz, JE, Taglialatela, G. Postsynaptic proteome of non-demented individuals with Alzheimer's neuropathology. [In preparation]
3. Fracassi, A, **Zolochevska, O,** Moreno, S, Taglialatela, G. Oxidative stress and antioxidant response in frontal cortex of demented and non-demented individuals with Alzheimer's neuropathology. [In preparation]

ACKNOWLEDGEMENTS

I would like to thank my mentor, Dr. Taglialatela, for his guidance during the years of my Ph.D. studies. I am indefinitely greatful for his support of all my professional and personal endeavors.

I would like to thank my science family for the insightful discussions, encouragement and sense of humor, which was greatly appreciated during the difficult times. Special thanks to Dr. David Briley, Dr. Claudia Marino and Whitney Franklin – your friendship added many bright colors to the routine. I also thank Michele Comerota, Salvo Saieva, Anna Fracassi, Wen Ru Zhang and Dr. Balaji Krishnan.

I would also like to thank my committee members: Drs. Maria Adelaide Micci, Rakez Kayed, John Wiktorowicz, Christopher Norris and Jere McBride.

Dr. David Niesel, Dr. Dorian Coppenhaver, Dr. Pomila Singh and Aurora Galvan at UTMB.

Dr. Francesco Cappello at UNIPA for his help and support.

Most importantly, I would like to thank my non-science family who had my back during these years. My husband, who had to suffer through proofreading of my abstracts and papers; who had to be the dog walker, the cook, the housekeeper and both mommy and daddy at times. My mom, who has been listening to my sciency monologues for many years and has not complained a single time. And last, but definitely not least, my daughter, the light of my life, who most likely will not remember mommy being in school, but hopefully will appreciate highly educated parents.

ABSTRACT

Some individuals, here refereed to as Non-Demented with Alzheimer's Neuropathology (NDAN), retain their congitive function despite the presence of amyloid plaques and tau tangles typical of symptomatic Alzheimer's Disease (AD). In NDAN, unlike AD, toxic amyloid beta oligomers do not localize to the postsynaptic densities (PSDs). Synaptic resistance to amyloid beta in NDAN may thus enable these individuals to remain cognitively intact despite the AD-like pathology. The mechanim(s) responsible for this resistance remains unresolved and understanding such protective biological processes could reveal novel targets for the development of effective treatments for AD. The current work describes the use of a proteomic approach to compare the hippocampal postsynaptic densities of NDAN, AD and healthy age-matched persons to identify protein signatures characteristic for these groups. Subcellular fractionation followed by 2D gel electrophoresis and mass spectrometry were used to analyze the PSDs. Fifteen proteins are identified as the unique proteomic signature of NDAN PSDs, thus setting them apart from control subjects and AD patients. Using Ingenuity Pathway Analysis several microRNAs were identified as potential upstream regulators of the observed changes in the postsynaptic proteome. MicroRNA-149, -4723 and -485 were confirmed to have differential expression in AD and NDAN hippocampi when compared to control. We hypothesize that that global action of selected miRNAs plays a role in resistance to Aβ oligomer binding and toxicity. MicroRNA levels were modulated using mimics and inhibitors *in vitro* and *in vivo*. Both experimental systems showed that modulation of selected microRNAs results in reduced Aβ oligomer binding to the cellular surface *in vitro* and *in vivo*. Taken together, our findings suggest that the unique protein signature at the NDAN PSDs is regulated by the selected microRNAs, while modulation of microRNA levels *in vitro* and *in vivo* has an effect on Aβ oligomer binding,

further suggesting that a unique regulation of microRNAs in the NDAN subjects could be responsible for protection of synapses from Aβ toxicity, thus contributing to retention of cognitive ability.

CHAPTER 1. Background

Alzheimer's Disease

Alzheimer's Disease (AD) is the most common form of dementia, affecting more than 5 million Americans [1]. Age is the greatest risk factor for Alzheimer's, and over one third of the people older than 85 have AD. Other risk factors include family history and genetics (apolipoprotein ε, APOE; amyloid precursor protein, APP; presenilin, PSEN1 and PSEN2), gender (females are more susceptible), brain injury, cardiovascular health, physical activity and social interaction [2-4]. While available therapies are palliative and only temporarily improve cognition, there are no treatments that target pathological changes of AD. Currently there are five FDA (Food and Drug Administration) approved medications that are used to modulate cholinergic and glutamatergic circuits affected in AD [5].

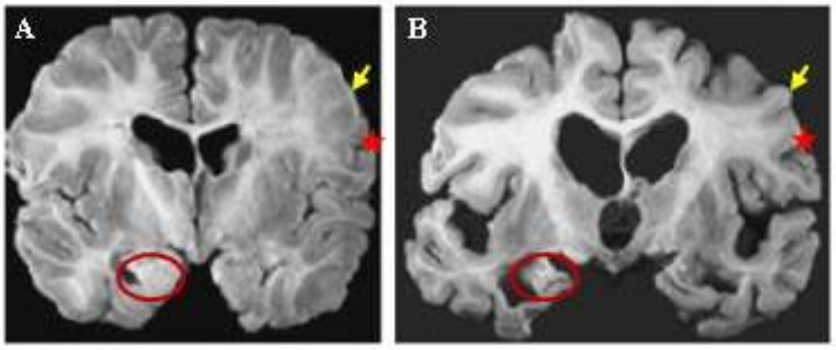

Figure 1.1. Coronal section of postmortem human brain. (A) Elderly nondemented individual, (B) AD patient. Widening of sulci (stars), shrinkage of gyri (arrows), significant shrinkage of hippocampus (circled) are typical changes during AD. Modified from Yaari and Corey-Bloom [6].

AD is a multifactorial disease that is characterized by cognitive decline and unique pathology. The brain atrophy (Fig. 1.1) with widening of sulci and shrinkage of gyri is observed in AD [6]. The hippocampus (Fig. 1.1, circled), responsible for formation of new memories, is one of the most affected areas in the brain [7].

Microscopic changes in the AD brain begin long before memory loss [8]. Synapse loss is believed to occur at early stages of the disease [6, 8], whereas cell death occurs at later stages and is directly related to cognitive decline [8]. Neurodegeneration in AD is linked to abnormal aggregation of proteins. Two main neurodegenerative processes in the AD brain are amyloidogenesis and neurofibrillary degeneration [9]. Amyloidogenesis leads to deposition of extracellular amyloid beta (Aβ) peptide, while neurofibrillary tangles (NFTs) contain hyperphosphorylated tau protein. However, there is no correlation between presence of mature Aβ deposits and NFTs with the cell loss or cognitive decline [3, 10-13]. On the other hand, presence of soluble oligomeric species of Aβ and tau in the brain correlates with cognitive dysfunction [11, 14-16]. Early oligomers formed during aggregation process, the most toxic forms of misfolded Aβ and tau, can accumulate at the synapse and synergistically impair dendritic spines in the hippocampus [11, 17-21]. Aβ and tau oligomer-driven toxicity may cause apoptosis, mitochondrial damage, disrupted Ca^{2+} homeostasis and toxic free radical formation [15, 22, 23]. Figure 1.2 shows a representative immunohistochemical detection of Aβ and NFTs.

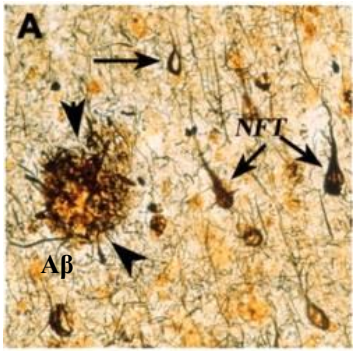

Figure 1.2. Pathology of AD. Aβ plaques (arrowheads) and neurofibrillary tangles (arrows) in AD brain are revealed by the Bielschowsky silver stain. Modified from Nixon [24].

AD is diagnosed through a series of medical tests which include assessment of mental status, physical and neurological exams, evaluation of medical history and additional tests (*e.g.* blood tests, brain imaging) [25]. One of the tests widely used in clinic is the Mini-Mental State Examination (MMSE), which assesses global cognitive function on a 0-30 scale (27-30 indicates a normal cognition) [26]. There is no single test to determine whether someone has Alzheimer's. Only at autopsy, neuropathologists can confirm AD diagnosis by evaluation of microscopic changes caused by the disease [27]. Based on the level of accumulation and distribution of NFTs, one of six Braak stages is assigned [28]. Braak I-II stages are characterized by changes in cortex, mild involvement of hippocampus and absence of isocortical changes. Mild to moderate damage of hippocampus and low isocortical involvement is typical for Braak III-IV. Stages V and VI are described by pathological changes in all components of hippocampus, isocortex, insula, orbitofrontal cortex, hypothalamus and substantia nigra [28].

Amyloidogenesis

Accumulation of Aβ in the brain is an important step in AD pathogenesis [3]. Amyloid precursor protein (APP) is a 770 amino acids long, 87 kDa type I transmembrane glycoprotein

(Fig. 1.3), which is ubiquitously expressed and evolutionary conserved [29]. APP_{770}, APP_{751} (primarily found in T-lymphocytes) and APP_{695} (predominantly neuronal) are three most abundant isoforms of APP [30].

APP is important in synaptic transmission, learning and memory, and synaptic plasticity [3, 31]. More than 20 years ago mutations in APP and APP-processing enzymes (PSEN1/PSEN2; integral membrane protein 2B, BRI2/ITM2B) were linked to familial AD [3, 31]. On the other hand, some polymorphisms in APP (for example, A673T) have a protective function against cognitive decline [32].

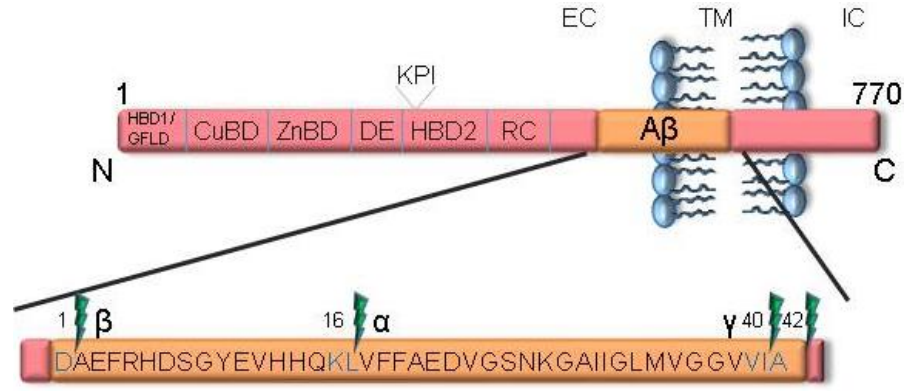

Figure 1.3. Functional domains of amyloid precursor protein. Extracellular (EC) APP domains include: heparin binding and growth factor like domain (HBD1/GFLD), copper binding domain (CuBD), zinc binding domain (ZnBD), acidic region (DE), second heparin binding domain (HBD2), Kunitz-type protease inhibitor domain (KPI, not present in APP_{695}), random coiled region (RC) and amyloid beta domain (Aβ). Sites of APP cleavage by α-, β- and γ-secretase are displayed in the inset. TM – transmembrane, IC – intracellular. Modified from Lazarov and Demars, Vetrivel and Thinakaran [30, 33].

APP can be cleaved by at least three enzymes: α-, β- and γ-secretases (Fig. 1.3, 1.4) [29, 30]. α-secretase cleaves within the Aβ sequence, generating non-toxic C83 (10 kDa membrane-

bound COOH-terminal domain) and soluble APPα (sAPPα, NH_2-terminal peptide). Thus, this type of cleavage is referred to as *Non-amyloidogenic pathway* (Fig. 1.4). In the *Amyloidogenic pathway*, two peptides form when APP is cleaved by β-secretase: C99 (12 kDa COOH-terminal peptide) and soluble APPβ (sAPPβ, ~100 kDa soluble NH2-terminal fragment). C99, further ceaved by γ-secretase at position 40 or 42, results in formation of Aβ (4 kDa peptide) and APP intracellular domain (AICD). γ-secretase has several recognition sites on Aβ peptide to yield 39-43 amino acid Aβ [34]. Two main forms of Aβ are Aβ40 and Aβ42, which have different COOH-termini. Aβ42 has been suggested to cause the familial early-onset AD [35].

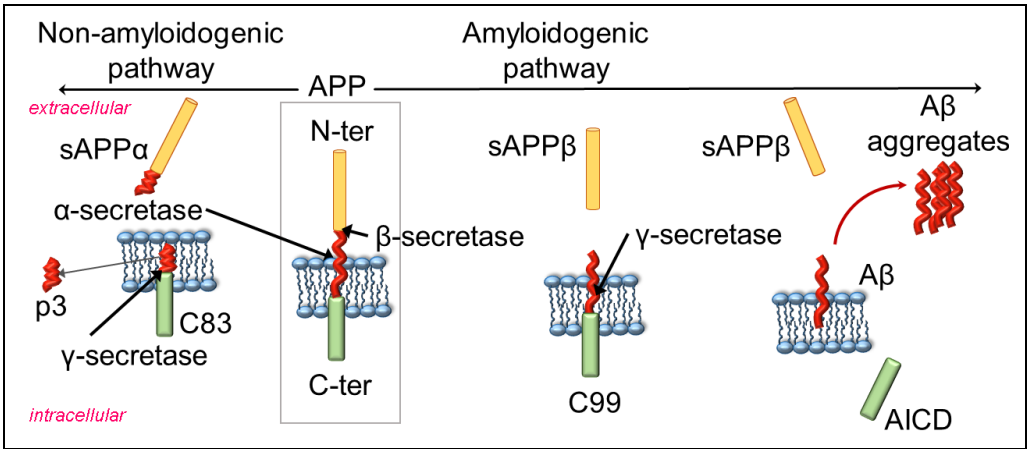

Figure 1.4. The amyloid precursos protein (APP) undergoes proteolytic cleavage by secretase enzymes. Combined cleavage of α- and γ-secretases produces soluble APP (sAPPα), C-terminal fragment (C83) and p3 preventing Aβ generation. β- and γ-secretases cleave APP to form APP intracellular domain (AICD), soluble APP (sAPPβ) and amyloidogenic Aβ. Modified from Picone, Cole and Vassar [9, 36].

The 4 kDa Aβ peptide, cleaved by β- and γ-secreatases, forms insoluble aggregates which are believed to cause neurodegeneration [36]. Misfolding of Aβ into toxic aggregates involves few steps: monomer → paranuclei or small oligomers → large oligomers → protofibrils (5 nm) → fibrils (10 nm) [14]. Early oligomers formed during aggregation, the most toxic form of

misfolded Aβ, can accumulate at the synapse [11, 17-19]. The toxicity may cause apoptosis, disrupted Ca^{2+} homeostasis and toxic free radical formation [22]. Synaptic dysfunction in AD is observed as a result of Aβ oligomers association with the PSD [19]. However, there is no correlation between presence of mature Aβ deposits and NFTs with cell loss or cognitive decline [3, 10-12]. On the other hand, presence of soluble Aβ (monomers and oligomers) in the brain correlates with cognitive dysfunction [11, 14]. Small Aβ oligomers (8 kDa dimers, 12 kDa trimers and 16 kDa tetramers) modify protein content at PSD inducing dendritic spine loss, and causing shrinkage of PSDs in cultured neurons [19, 37]. Size of PSD is proportional to the synapse strength, and therefore, Aβ-driven synapse damage can result in the loss of cognitive function.

Non-Demented with Alzheimer's Neuropathology

AD has a long asymptomatic stage, and with the development of neuroimaging it is becoming more clear that some individuals with AD-like neuropathology (Fig. 1.5) do not exibit any cognitive decline during their life [8, 12, 38]. However, it is unknown if these individuals will develop dementia later in life. Alzheimer's Association workgroup in the diagnostic guidelines for Alzherimer's Disease, part of National Institute on Aging, developed research recommendations for the study of cognitively intact indivuals with typical AD neuropathology. Such individuals can be described as "asymptomatic at risk for AD dementia", or "not normal, not MCI [Mild Cognitive Impairment]" [38]. In our laboratory we refer to this cohort of individuals as Non-Demented with Alzheimer's Neuropathology (NDAN) [39, 40]. Several

research groups, including ours, are trying to understand the mechanisms involved in preservation of cognition in people with high levels of Aβ plaques and NFTs [3, 12, 38-47].

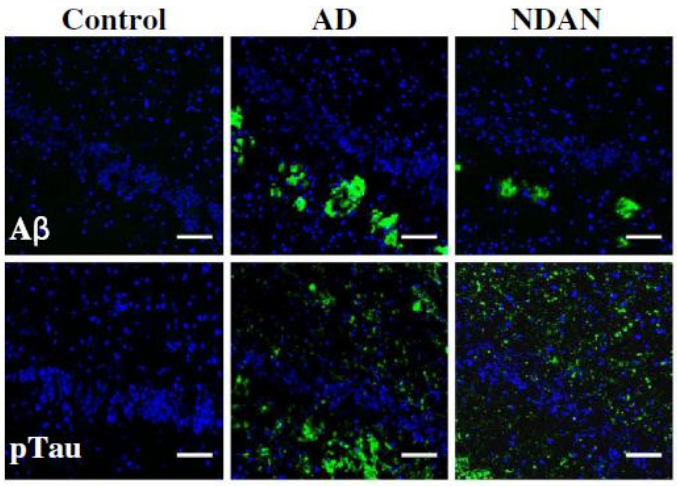

Figure 1.5. Immunohistochemical staining of control, AD and NDAN hippocampi. Data from our laboratory demonstrating Aβ plaques (top row) and phosphorylated tau (bottom row) in dentate gyrus of individuals classified as control (Braak 1, Plaque 3, MMSE 30), AD (Braak 6, Plaque 1, MMSE 2), or NDAN (Braak 6, Plaque 1, MMSE 27). DAPI-containing mounting medium was used to visualize nuclei (blue). 20x magnification, scale bar 100 µm [39].

One of the hypotheses is that presence of AD lesions in the brain may not be sufficient to cause cognitive decline in these individuals due to larger brain reserve [41]. Total brain and hippocampal volume were shown to be greater in cognitively intact subjects with high load of Aβ plaques and NFTs [8]. Additionally, higher number of synapses and enlargement of neuronal nuclei are hypothesized to correlate with preserved cognitive function [41, 42, 46]. Cell loss has been observed in AD patients, therefore different apoptosis regulation in cognitively normal humans can play a role in resistance to dementia [41]. Insulin degrading enzyme was found to be

increased in AD when compared to NDAN, which suggests that degradation of insulin is increased in AD, therefore, glucose is less available to the brain cells [3]. Additionally, insulin prevents binding of Aβ oligomers to the synapse thus improving cognitive performance in patients with early AD [48, 49]. Insulin-resistant type II diabetes patients are at a higher risk for development of Alzheimer's; induction of diabetes in mouse models of AD leads to cognitive decline and loss of synapses [48].

Aβ interaction with postsynaptic density

The loss of synapses has been reported to relate to cognitive decline observed during AD progression [50]. The mechanism of Aβ synaptotoxicity is not fully understood, but it is hypothesized that Aβ oligomer association with PSD results in disturbed Ca^{2+} signaling in dendritic spines, which can affect multiple downstream pathways [37]. For example, injection of Aβ oligomers into the CNS blocks long-term potentiation and disrupts cognitive function in rats [50]. We have previously published that, contrary to Aβ oligomers, fibrillar Aβ is incapable of association with the PSD of primary hippocampal neurons (Fig. 1.6A) [37]. Aβ oligomers can interact with multiple proteins and receptors at the PSD, for instance, α7-nAChR (α7-nicotinic acetylcholine receptor), AChE (acetylcholinesterase), PrPc (prion protein), NMDAR (N-methyl-D-aspartate receptor), TNF-R (tumor necrosis factor receptor), α2β1 and αVβ1 integrins, NL-1 (neuroligin-1) and others [50].

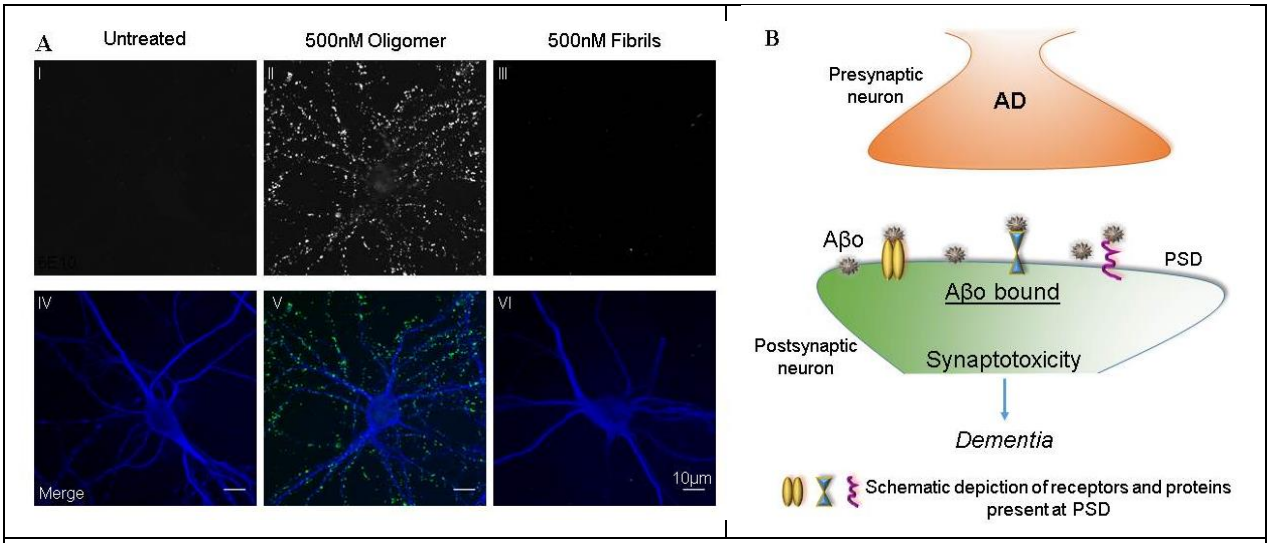

Figure 1.6. Aβ oligomers bind AD hippocampal synapses. (A) Oligomeric, but not fibrillar Aβ associates with dendritic processes of primary hippocampal neurons. Rat primary hippocampal neurons (day 17) were exposed to 500 nM oligomers or 500 nM fibrils (prepared in our laboratory) for 60 minutes then fixed and immunolabeled using 6E10 (green), which recognizes Aβ (I-III) and MAP2 (microtubule-associated protein 2; blue) antibodies. Merge is shown in (IV-VI) [37]. (B) Diagrammatic representation of Aβ oligomers (Aβo) binding to the PSD in AD results in synaptic dysfunction. Modified from Bjorklund *et al.* [39]

Synaptic dysfunction in AD is observed as a result of Aβ oligomers association with the PSD (Fig. 1.6B) [19]. Small Aβ oligomers (8 kDa dimers, 12 kDa trimers and 16 kDa tetramers) modify protein content at PSD inducing dendritic spine loss, and causing shrinkage of PSDs in cultured neurons [19, 37]. Size of PSD is proportional to the synapse strength, and therefore, Aβ-driven synapse damage can result in the loss of cognitive function. Plasticity and cognition is affected through the perturbation of Ca^{2+}/calmodulin-dependent protein kinase II-α (CaMKII) autophosphorylation [37].

Plasticity and cognition is affected through the perturbation of Ca^{2+}/calmodulin-dependent protein kinase II-α (CaMKII) autophosphorylation [37]. We have established that oligomers, but not fibrills, decrease CaMKII autophosphorylation in hippocampal synapses, which can be used as a "molecular read-out for patient symptoms" [37]. Association of Aβ

oligomers with the PSD implicates dephosphorylation (deactivation) of CREB (cAMP response element-binding protein factor), which in turn affects transcription of genes regulating long-term changes in synaptic strength [51].

NDAN synapses reject Aβ, which could explain why NDAN subjects remain cognitively intact. In fact, our laboratory has demonstrated for the first time that the PSD of NDAN subjects is free of Aβ oligomers (Fig. 1.7A, B) [39].

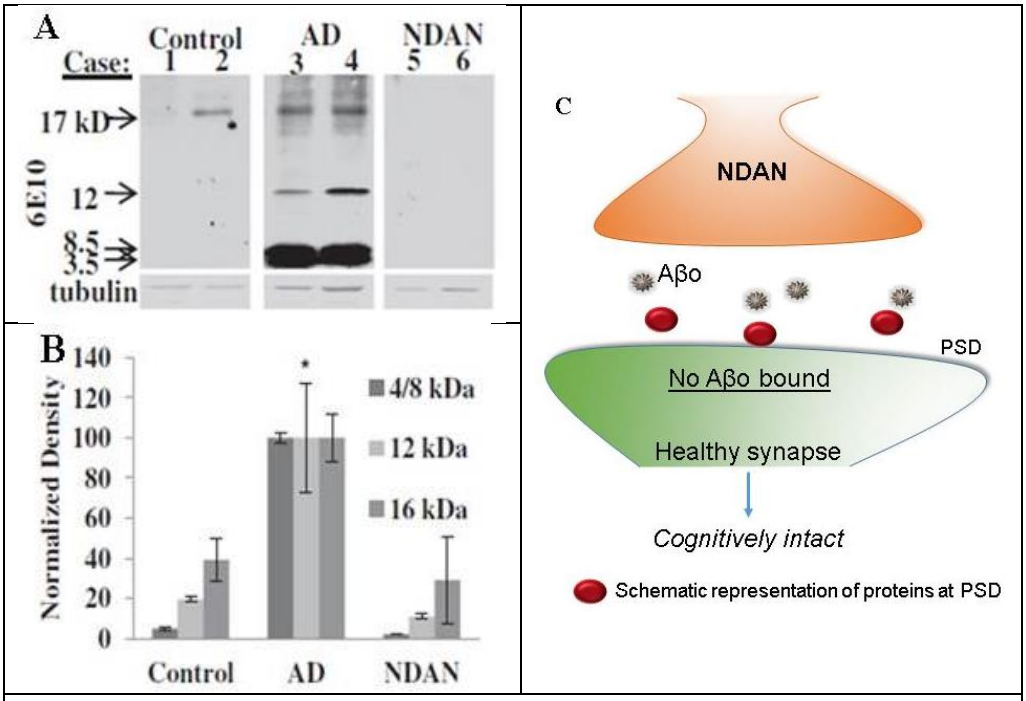

Figure 1.7. The Aβ oligomer rejection by post-synaptic density in NDAN subjects. (A) Hippocampi from six different patients were evaluated for low molecular weight Aβ association synapses (40 µg protein each lane of a 10-20% tris-glycine gradient gel) [39]. (B) Densitometric analysis of each of the Aβ species (monomer/dimer = 4-8.5 kDa band, trimer = 12 kDa, and tetramer = 16 kDa) demonstrates that all Aβ species are increased in AD. The results are expressed as the mean ± SEM using propagation of error and normalized with AD = 100%. The asterisk denotes the values significantly higher than control (monomer/dimer, p = 0.012, trimer, p =< 0.001, and tetramer, p = 0.014; ANOVA; a Bonferroni correction was required for the monomer/dimer and trimer density values) [39]. (C) Diagrammatic representation of Aβ oligomers (Aβo) at the PSD of NDAN subjects. Red spheres represent unique protein signature, involved in Aβo rejection. Modified from Bjorklund *et al.* [39]

The underpinning mechanism affording the synapse this extraordinary resistance to Aβ oligomers remains unknown. Based on this observation, we **hypothesize** that there is a unique protein set at the PSD of NDAN subjects that can be involved in Aβ rejection by synapses (Fig. 1.7C; data supporting this hypothesis is discussed in Chapter 2). To the best of our knowledge, there is no published evidence that explains the mechanisms of Aβ rejection in NDAN synapses. Understanding such mechanism is the main goal of the present project.

AIM OF THE DISSERTATION

Alzheimer's disease (AD) is the 6th leading cause of death in the US, affecting more than 5.3 million Americans [1]. AD is characterized by the CNS accumulation of extracellular Aβ aggregates and hyperphosphorylated tau-containing intracellular NFTs. AD is also accompanied by the loss of synapses and later by overt neuronal death [52]. Current treatments address symptoms of the disease with limited efficacy, and there is no pharmacological therapy to prevent or stop the progression of AD.

In recent years, several research groups have described individuals that remain cognitively intact in spite of having accumulation of Aβ and NFTs (seen in fully symptomatic AD) [41-43, 46] – "Non-Demented with Alzheimer's Neuropathology" (NDAN) ([39], reviewed in [53]). Unveiling the yet unclear mechanisms responsible for preservation of cognitive function in NDAN is important as it would support a new treatment strategy centered on inducing cognitive resistance in anyone affected by AD. Unlike AD patients, NDAN show little or no synapse loss [54]. Bjorklund *et al.* have previously reported that the post-synaptic density (PSD) of NDAN subjects is resistant to Aβ binding, therefore protecting synapses and likely contributing to maintenance of cognitive ability despite the presence of AD neuropathology [39]. The central hypothesis of this project is that the post-synaptic density of NDAN subjects has a unique protein signature that protects synapses from detrimental binding of Aβ. I further hypothesize that miRNAs play an important role in determining such extent of synaptic function and synaptic integrity.

In order to test the main hypothesis, the proteomics of PSD fractions of hippocampi of control (non-demented, age-matched), AD and NDAN was performed (Chapter 2). Specific

miRNAs were identified as potential drivers of the protein signature observed at NDAN PSD. In Chapter 3 I describe three miRNAs and their role in Aβ oligomer binding to the synapses.

The work described here addresses a previously unappreciated unique phenomenon – an exceptional ability to resist cognitive decline despite the presence of AD pathology.

CHAPTER 2. Synaptic Proteome

Background

Synaptic dysfunction in AD is observed as a result of Aβ oligomers association with the PSD [19]. At the PSD, Aβ oligomers oppose expression of long-term potentiation (LTP), modify protein content and induce dendritic spine shrinkage and eventually loss [19, 22, 37]. Since the size of the PSD is proportional to the strengh of the synapse, Aβ-driven synapse damage can result in the loss of cognitive function. In AD, plasticity and cognition are affected through the perturbation of Ca^{2+}/calmodulin-dependent protein kinase II-α (CaMKII) autophosphorylation [37]. Association of Aβ oligomers with the PSD implicates dephosphorylation (deactivation) of CREB (cAMP response element-binding protein factor), which in turn affects transcription of genes regulating long-term changes in synaptic strength [51].

We have previously reported that NDAN synapses reject Aβ oligomers, which could explain why NDAN subjects remain cognitively intact. Our laboratory has demonstrated for the first time that the PSDs of NDAN subjects are free of Aβ oligomers [39]. Based on this observation, I hypothesized that there might be unique changes in protein expression levels at the PSDs of NDAN subjects that specifically mark the ability of their PSDs in the hippocampus to reject binding of toxic Aβ oligomers. To test this hypothesis, in the present work I performed proteomic anaysis of the PSDs isolated from healthy control, AD and NDAN individuals. The protein levels in AD and NDAN were compared to control, in addition to direct NDAN vs. AD comparison. As a result, I identified a unique PSD protein signature of NDAN which consists of fifteen proteins, setting them apart from control and AD.

Methods

Case subjects

Frozen mid-hippocampus tissue was obtained from the Oregon Brain Bank at Oregon Health and Science University (OHSU) in Portland, OR. Donor subjects were enrolled and clinically evaluated in studies at the NIH-sponsored Layton Aging and AD Center (ADC) at OHSU. Subjects were participants in brain aging studies at the ADC and received annual neurological and neuropsychological evaluations, with a clinical dementia rating (CDR) assigned by an experienced clinician. Controls had normal cognitive and functional examinations. The AD subjects were diagnosed by a clinical team consensus conference, met the National Institute for Neurological and Communicative Disorders and Stroke-Alzheimer's Disease and Related Disorder Association diagnostic criteria for clinical AD, had a CDR of greater than 1.0 and neuropathologic confirmation at autopsy (after informed consent). Tissue use conformed to institutional review board-approved protocols. Neuropathologic assessment conformed to National Institute on Aging-Reagan consensus criteria. All brain tissue was examined by a neuropathologist for neurodegenerative pathology including neurofibrillary tangles and neuritic plaques. Using standardized CERAD criteria [55], cases were assigned an amyloid score based on the deposition of amyloid plaques in the brain (0 = no plaques, 1 = sparse plaques, 2 = moderate plaques and 3 = dense plaques) and a Braak stage (0–6; with 6 being the most severe) indicative of the level and location of hyperphosphorylated tau tangles [28]. In addition to the pathological information detailed above, demographical data were received along with the frozen tissue. These included age, sex and MMSE score [55] for each case.

Synaptic fractionation

Synaptic fractionation was performed as described previously [56, 57]. Briefly, hippocampal tissue was homogenized using a Dounce glass homogenizer and synaptosomes were isolated using a sucrose gradient and ultracentrifugation (100,000 x g for 3 h at 4°C). Synaptic junctions were obtained by incubating the synaptosomes in pH = 6 buffer (1 M Tris in 0.1 mM $CaCl_2$) and then centrifuging at 40,000 x g for 30 min at 4°C. The supernatant (containing synaptic vesicles) and the pellet were collected separately. The pellet was solublized and incubated in pH = 8 buffer (20 mM Tris, 1% Triton X-100 in 0.1 mM $CaCl_2$) and then centrifuged at 40,000 x g for 30 min at 4°C to generate the PSD pellet. This pellet was solublized in 1% SDS. Eight samples per group were pooled for analysis.

Proteomics

Control, NDAN and AD samples were processed for proteomic analysis as described previously [for examples, see 58, 59]. Triplicate samples from control, AD and NDAN PSD (200 µg) were extracted with 7M urea, 2M thiourea, 2% CHAPS and 50mM Tris pH 7.5, treated with sodium ascorbate (Asc) to reverse S-nitrosylation and then dialyzed against the urea buffer to remove Asc, which interferes with labeling. Protein concentrations were determined with the Lowry method and cysteines (cysteic acid) determined by amino acid analysis (Model L8800, Hitachi High Technologies America, Pleasanton, CA, USA). Proteins from the tissues were then labeled with BODIPY® FL *N*- (2-aminoethyl) maleimide (Life Technologies, Inc., Carlsbad, CA, USA) at 60-fold excess cysteine to BODIPY FL-maleimide (BD, San Jose, CA, USA) as

published previously [60]. After quenching the labeling reactions with 10x molar excess β-mercaptoethanol (BD: βME), 200 µg labeled proteins in 0.5% IPG buffer pH3-10 (GE Healthcare, Pittsburg, PA, USA) were loaded onto a 11cm pH 3-10 IPG strip (GE Healthcare, Pittsburg, PA, USA) and proteins were focused according to the previously published protocol [61]. After focusing, the IPG strips were equilibrated in 6M Urea, 2% SDS, 50mM Tris, pH 8.8, 20% glycerol for 30 min at room temperature, applied to an 8-16% Tris-glycine-SDS gel and run at 150V x 2.25 hr at 4°C. The gels were fixed for 1 hr in 10% methanol, 7% acetic acid and washed overnight in 10% ethanol. Finally, gels were imaged on a Typhoon Trio Imaging System (GE Healthcare; excitation λ = 480/40 nm & emission λ = 535/50 nm). It was previously demonstrated that this covalent sulfhydryl alkylation method using an uncharged thiol-reactive dye exhibits excellent specificity for cysteine thiols – little to no modification of other amino acid residues, does not impact protein electrophoretic mobility – for spot matching with unlabeled proteins, and accomplishes highly accurate and reproducible quantification – by virtue of its specificity and saturating concentration over protein thiols [58, 60].

Protein quantification and image analysis

The 2D gel electrophoresis (2DE) images were analyzed using SameSpots software (TotalLab, Ltd. Newcastle Upon Tyne, UK). The software performs pixel-to-pixel matching before spot detection, ensuring that spot boundaries are the same for all gels, and eliminating errors that accumulate in the reference gel(s) as the number of gels within one experiment increases. Once the pixel matching and spot detection is complete, a reference gel is selected according to several criteria, including quality and number of spots. Subsequent to automatic

spot detection, spot filtering is manually performed and spots with an area of less than 250 pixels are filtered out, and spots with a volume (intensity) / area ratio of less than 375 pixels (whose abundance is insufficient for mass spectrometry (MS) identification) are also filtered. Typically, some manual spot editing is required to correct for spots that are not split correctly, not detected, or split unnecessarily during the automated detection process. The matching of spots between the gels is manually reviewed and adjusted as necessary. The software normalizes spot volumes using a calculated bias value based on the assumption that the great majority of spot volumes represent no change in abundance (ratio control to experimental = 1.0) (TotalLab documentation).

Ratiometric calculation from BODIPY-fluorescence units was conducted for quantifying differential protein abundance for the samples, and parametric t-test performed on log 2 normalized abundance ratios.

Mass spectrometry and protein identification

Selected 2DE spots that exhibited significant differential prevalence ($p \leq 0.05$) were picked robotically (ProPick II, Digilab, Ann Arbor, MI, USA), and trypsin digested. In brief, gel spots were incubated at 37°C for 30 min in 50 mM NH_4HCO_3, dehydrated twice for 5 min each in 100 µl acetonitrile, dried, and proteins were digested in-gel at 37°C overnight with 10 µl of trypsin solution (1% trypsin in 25 mM ammonium bicarbonate). Peptide mixtures (1 µl), obtained after tryptic digestion, were directly spotted onto a target plate with 1 µl of alpha-cyano-4-hydroxycinnamic acid matrix solution (5 mg/ml in 50% acetonitrile) and analyzed by matrix assisted laser desorption ionization-time of flight (MALDI-TOF/TOF) MS using the ABI

4800 Proteomics Analyzer (AB Sciex, Foster City, CA, USA). The Applied Biosystems software package included the 4000 Series Explorer (v.3.6 RC1) with Oracle Database Schema (v.3.19.0) and Data Version (3.80.0) to acquire and analyze MS and MS/MS spectral data. The instrument was operated in a positive ion reflectron mode with the focus mass set at 1700 Da (mass range: 850-3000 Da). For MS data, 1000-2000 laser shots were acquired and averaged from each protein spot. Automatic external calibration was performed by using a peptide mixture with the reference masses 904.468, 1296.685, 1570.677, and 2465.199. Following MALDI MS analysis, MALDI MS/MS was performed on several (5-10) abundant ions from each protein spot. A 1 kV positive ion MS/MS method was used to acquire data under post-source decay (PSD) conditions. The instrument precursor selection window was +/- 3 Da. Automatic external calibration was performed by using reference fragment masses 175.120, 480.257, 684.347, 1056.475, and 1441.635 (from precursor mass 1570.700).

AB Sciex GPS Explorer^{TM} (v.3.6) software was employed in conjunction with MASCOT (v.2.2.07) to search the UniProt human protein database (last accessed: June 7, 2015; 87,656 sequences 35,208,664 residues) by using both MS and MS/MS spectral data for protein identification. Protein match probabilities were determined by using expectation values and/or MASCOT protein scores. The MS peak filtering included the following parameters: a mass range of 800 Da to 3000 Da, minimum S/N filter = 10, mass exclusion list tolerance = 0.5 Da, and mass exclusion list for some trypsin and keratin-containing compounds included masses (Da) 842.51, 870.45, 1045.56, 1179.60, 1277.71, 1475.79, and 2211.1. The MS/MS peak filtering included the following parameters: minimum S/N filter = 10, maximum missed cleavages = 1, fixed modification of carbamidomethyl (C), variable modifications due to oxidation (M), precursor tolerance = 0.2 Da, MS/MS fragment tolerance = 0.3 Da, mass = monoisotopic, and

peptide charges = +1. The significance of a protein match, based on the peptide mass fingerprint (PMF) in the MS and the MS/MS data from several precursor ions, is presented as expectation values ($p < 0.001$).

In addition, where MALDI protein confidence scores left ambiguous identification, the trypsin digested protein spots were analyzed by nano-LC-MS/MS using a Thermo Scientific Orbitrap Fusion MS (San Jose, CA, USA), coupled with a Dionex Ultimat 3000 nanoHPLC with a 40 well standard auto sampler. The samples were injected onto a nanotrap (100 µm i.d. x 1 cm, C18 PepMap 100), followed by a C18 reversed-phase (RP) home-packed column (SB-C18, ZORBAX, 5 micron from Agilent; Santa Clara, CA) at a flow rate of 400 nL/min with 60 min LC gradient (5% AcN, 0.1% trifluoroacetic acid (TFA) to 100% AcN, 0.1% TFA). The RP column was further eluted for several min with 90% AcN and TFA to minimize intersample contamination. Mass spectrometer parameters include the following: spray tip voltage at +2.2 kV, Fourier-transform MS mode for MS acquisition of precursor ions (resolution 120,000); ITMS mode for subsequent MS/MS of top 10 precursors selected; same ions were excluded for 15 sec; MS/MS was accomplished via collision induced dissociation.

Data analysis was performed using the MASCOT server by interrogating the total organism database. The selected analytical parameters included: the enzyme as trypsin; maximum missed cleavages = 2; variable modifications included oxidation (methionine); precursor ion mass tolerance was set at 5 ppm; fragment ion mass tolerance was 0.6 Da. The significance of a protein match is based on peptide expectation values and the numbers of peptides found (≥ 2). The default significance threshold is $p \leq 0.05$ to achieve a false discovery rate (FDR) of less than 1.0%. Protein identifications were accepted if they could be established at 95.0% probability to achieve an FDR [62] of less than 1.0%.

Results

Proteins identified

The goal of this study was to determine if the unique ability of NDAN postsynaptic densities (PSDs) to reject Aβ oligomer binding can be explained by a unique protein signature that sets NDAN aside from AD and healthy age-matched control individuals. PSD fractions from three experimental groups (control, AD and NDAN) were used in a discovery-mode proteomics, the cases were pooled in order to increase the likelihood that the proteins identified would be universal to the experimental group, while decreasing the inter-individual variability. Case subject data is provided in Table 2.1. In order to analyze the PSD proteome we determined the ratios of expression levels in three different ways: AD vs. control, NDAN vs. control and NDAN vs. AD.

Seven hundred and twenty-seven individual spots were detected on Coomassie-stained 2DE of isolated PSDs (Fig. 2.1). Three hundred and forty most abundant spots were collected for protein digestion. Following digestion, the resulting peptides were separated by liquid chromatography and the amino acid sequences were determined. Using MS/MS we identified 122 proteins that have the p-value ≤ 0.05 in at least one comparison (*i.e.* AD vs. control, NDAN vs. control, or NDAN vs. AD) and MALDI protein score cut-off ≥ 62.

Case number	Diagnosis	Age	Sex	PMI, hrs	Braak	MMSE
1525	Control	89	F	3	1	29
1716	Control	>89	M	4.5	1	29
1944	Control	>89	F	8	4	29
1957	Control	>89	F	8	4	30
1965	Control	>89	F	5.5	2	26
1977	Control	>89	F	4	4	28
2337	Control	86	M	16.5	4	26
2376	Control	>89	M	4	4	30
1791	AD	>89	M	10	4	19
2010	AD	87	F	6	3	23
2126	AD	>89	F	9	3	26
2146	AD	>89	F	9.5	3	30
2157	AD	>89	M	11.5	4	12
2221	AD	>89	F	15.5	4	29
2315	AD	>89	M	4	4	28
2330	AD	>89	F	4.5	4	28
697	NDAN	>89	M	5	5	29
1095	NDAN	88	M	3	4	29
1179	NDAN	89	F	2.5	5	27
1362	NDAN	>89	F	48	4	27
1644	NDAN	76	F	30	5	30
1677	NDAN	>89	F	18	6	30
1686	NDAN	87	F	2.5	2	29
1845	NDAN	86	M	4.5	4	29

Table 2.1. Demographic data of the cases used in the present study. PMI – post-mortem interval, MMSE – mini-mental state exam.

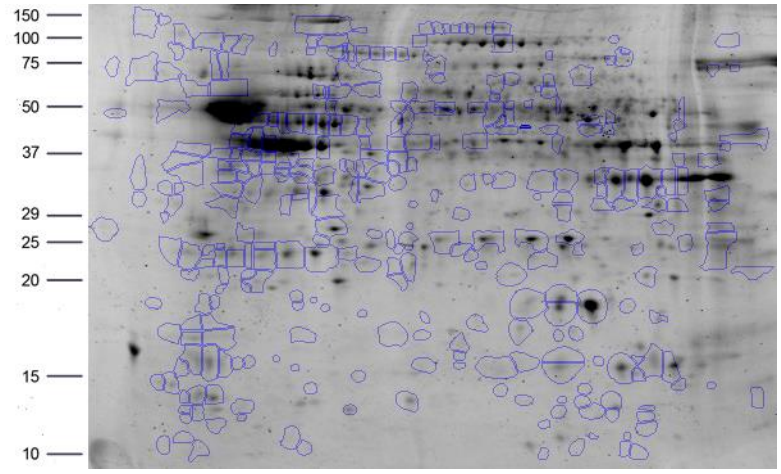

Figure 2.1. Representative 2DE of proteins identified. The highlighted spots were excised and analyzed in the present study. The x-axis is calibrated in pH units, while y-axis is calibrated in mass units (kDa).

In the Supplementary table 1 there are 10 additional proteins that presented with the p-values greater than 0.05, however, are relevant and contribute to the discussion. Since the goal of this work was to determine differences between AD and NDAN that would reflect their diverse cognitive status and synaptic vulnerability to Aβ oligomers, we selected proteins that were statistically changed (cut-off ≥ ±1.5 fold) in NDAN vs. AD, regardless of whether they were changed in either group as compared to controls. Following this criterion, thirty-one proteins with the fold change of at least ±1.5 in NDAN vs. AD were chosen for further analysis (Table 2.2).

Protein name	Gene ID	Accession Number	Theoretical pI	Measured pI	Theoretical Mw,	Measured Mw,	MS ID protein score	AD vs. control	p-value	NDAN vs. AD	p-value	NDAN vs. control	p-value
Actin, cytoplasmic 2	ACTG1	P63261	5.31	6.31	42	15	78	-1.50	0.170	-1.49	0.351	-2.23	0.029
Annexin (Fragment)	ANXA2	H0YN42	5.56	8.03	29	30	141	1.55	0.404	1.83	0.358	2.85	0.099
Calcium/calmodulin-dependent protein	CAMK2A	Q9UQM7	6.61	5.84	54	17	115	1.43	0.452	1.98	0.143	2.83	0.041
Calreticulin	CALR	P27797	4.29	4.65	48	71	70	-1.15	0.335	-2.85	0.001	-3.27	0.000
Creatine kinase B-type	CKB	P12277	4.29	6.93	48	17	70	1.05	0.596	-1.98	0.001	-1.88	0.003
Creatine kinase B-type (Fragment)	CKB	G3V4N7	4.89	5	24	20	116	1.09	0.415	-2.80	0.003	-2.57	0.004
Glial fibrillary acidic protein	GFAP	P14136	5.42	5.39	50	46	1010	-1.44	0.013	2.58	0.001	1.79	0.000
Glial fibrillary acidic protein	GFAP	P14136	5.42	5.34	50	46	950	-1.23	0.145	2.18	0.001	1.77	0.003
Glial fibrillary acidic protein	GFAP	P14136	5.42	5.28	50	46	969	-1.32	0.440	2.15	0.010	1.63	0.108
Glial fibrillary acidic protein	GFAP	P14136	5.42	5.43	50	46	1050	-1.25	0.175	2.12	0.004	1.69	0.024
Glial fibrillary acidic protein	GFAP	P14136	5.42	5.18	50	46	863	-1.02	0.925	2.06	0.006	2.02	0.007
Glial fibrillary acidic protein	GFAP	P14136	5.42	5.07	50	37	915	-1.48	0.001	1.53	0.001	1.03	0.587
Glial fibrillary acidic protein	GFAP	E9PAX3	5.42	4.98	50	18	374	1.27	0.234	-1.98	0.022	-1.56	0.192
Glial fibrillary acidic protein	GFAP	P14136	5.42	5.06	50	34	850	-1.44	0.030	-2.07	0.079	-2.97	0.027
Glial fibrillary acidic protein	GFAP	E9PAX3	5.42	5	50	20	400	-1.12	0.366	-4.32	0.006	-4.84	0.004
Glial fibrillary acidic protein (Fragment)	GFAP	K7EJU1	5.6	5.61	28	21	339	-4.13	0.009	2.00	0.196	-2.07	0.073
Glyceraldehyde-3-phosphate	GAPDH	E7EUT4	8.57	9.17	36	32	88	-6.19	0.141	6.55	0.149	1.06	0.990
Hemoglobin subunit beta	HBB	P68871	6.74	7.35	16	13	170	1.26	0.506	2.90	0.016	3.66	0.001
Hemoglobin subunit beta	HBB	P68871	6.74	7	16	14	70	1.68	0.071	1.84	0.182	3.09	0.043
Hemoglobin subunit beta	HBB	P68871	6.74	7.34	16	14	212	1.75	0.092	1.67	0.212	2.92	0.034
Isoform 1 of Vinculin	VCL	P18206-2	5.83	5.88	117	118	322	1.03	0.864	1.92	0.124	1.97	0.020
Isoform 2 of Glial fibrillary acidic protein	GFAP	P14136-2	5.42	5.09	50	36	223	-2.19	0.036	2.42	0.027	1.10	0.639
Isoform 2 of Glial fibrillary acidic protein	GFAP	P14136-2	5.42	5.16	50	35	92	-1.91	0.002	1.70	0.002	-1.12	0.175
Isoform 2 of Glial fibrillary acidic protein	GFAP	P14136-2	5.42	5.17	50	38	885	-1.12	0.100	1.63	0.016	1.46	0.045
Isoform 2 of Glial fibrillary acidic protein	GFAP	P14136-2	5.42	5.23	50	46	945	1.02	0.856	1.63	0.017	1.66	0.033
Isoform 2 of Glial fibrillary acidic protein	GFAP	P14136-2	5.42	5.5	50	46	974	-1.08	0.550	1.60	0.047	1.48	0.029
Isoform 2 of Glial fibrillary acidic protein	GFAP	P14136-2	5.42	5.07	50	37	790	-1.53	0.009	1.56	0.006	1.02	0.726
Isoform 2 of Glial fibrillary acidic protein	GFAP	P14136-2	5.42	5.16	50	49	828	-1.19	0.337	1.53	0.040	1.28	0.139
Isoform 2 of Glial fibrillary acidic protein	GFAP	P14136-2	5.42	5.74	50	48	284	2.04	0.041	-1.60	0.157	1.27	0.292
Isoform 3 of Dynamin-1	DNM1	Q05193-3	6.57	4.93	96	20	346	-1.23	0.257	1.69	0.016	1.38	0.094
Isoform 3 of Dynamin-1	DNM1	Q05193-3	6.57	4.88	96	19	300	-1.35	0.015	-1.60	0.016	-2.16	0.001
Isoform 3 of Peroxiredoxin-5, mitochondrial	PRDX5	P30044-3	9.12	7.7	17	15	154	1.29	0.081	-1.77	0.009	-1.37	0.005
Isoform 3 of Ras-related protein Rap-1b	PAR1B	P61224-3	8.72	6.37	19	19	112	-1.19	0.034	1.92	0.006	1.62	0.015
Isoform CNPI of 2',3'-cyclic-nucleotide 3'-phosphodiesterase	CNP	P09543-2	8.73	9.11	45	40	97	-1.66	0.127	1.82	0.293	1.10	0.970
Isoform Cytoplasmic+peroxisomal of Peroxiredoxin-5, mitochondrial	PRDX5	P30044-2	6.73	7.75	17	16	143	1.31	0.335	-2.27	0.088	-1.73	0.123
Isoform IB of Synapsin-1	SYN1	P17600-2	9.88	9.17	70	75	271	1.16	0.173	-1.72	0.001	-1.48	0.005
Isoform IB of Synapsin-1	SYN1	P17600-2	9.88	8.87	70	74	290	1.17	0.376	-2.00	0.032	-1.71	0.056
Isoform Non-brain of Clathrin light chain A	CLTA	P09496-2	4.45	4.69	24	30	62	-1.01	0.933	-3.31	0.005	-3.34	0.004
Keratin, type I cytoskeletal 10	KRT10	P13645	5.13	5.33	59	102	78	-1.04	0.794	-1.80	0.019	-1.87	0.018
Keratin, type I cytoskeletal 9	KRT9	P35527	5.14	6.14	62	17	95	-1.37	0.076	1.55	0.072	1.13	0.469
Keratin, type I cytoskeletal 9	KRT9	P35527	5.14	4.82	62	13	213	-1.21	0.405	-1.56	0.179	-1.89	0.046
Keratin, type II cytoskeletal 1	KRT1	P04264	8.15	7.55	66	12	181	1.32	0.067	-1.54	0.105	-1.17	0.447
Keratin, type II cytoskeletal 1	KRT1	P04264	8.15	4.66	66	35	63	-1.14	0.118	-1.81	0.001	-2.07	0.000
Keratin, type II cytoskeletal 1	KRT1	P04264	8.15	5.54	66	17	130	1.33	0.811	-3.10	0.370	-2.33	0.022
Malate dehydrogenase, mitochondrial	MDH2	P40926	8.92	8.94	36	30	228	1.67	0.005	1.77	0.102	2.97	0.016
NADH dehydrogenase [ubiquinone] 1 alpha subcomplex subunit 5	NDUFA5	F8WAS3	5.75	5.5	13	13	237	-3.21	0.134	-1.44	0.869	-4.62	0.040
NADH dehydrogenase [ubiquinone] flavoprotein 1, mitochondrial (Fragment)	NDUFV1	E9PQP1	8.51	8.26	51	46	105	2.77	0.003	-1.47	0.208	1.88	0.195
Neurofilament medium polypeptide	NEFM	E7EMV2	4.76	5.4	79	50	210	-1.28	0.321	1.50	0.241	1.17	0.635
Profilin-2	PFN2	C9J0J7	9.26	5.76	10	14	126	1.80	0.523	-1.54	0.684	1.17	0.554
Profilin-2	PFN2	C9J0J7	9.26	5.06	10	13	78	1.01	0.929	-2.08	0.047	-2.06	0.026
Pyruvate carboxylase, mitochondrial	PC	P11498	6.37	6.28	130	119	96	1.12	0.577	-1.59	0.048	-1.42	0.042
Rho GDP-dissociation inhibitor 1 (Fragment)	ARHGDIA	J3KTF8	5.37	5.02	22	20	185	1.18	0.094	-1.77	0.009	-1.50	0.033
Septin-7	SEPT7	F5GZE5	8.76	8.68	51	45	84	1.48	0.336	-1.66	0.075	-1.12	0.908
Spectrin alpha chain, non-erythrocytic 1	SPTAN1	Q13813	5.22	5.38	285	134	439	1.22	0.465	-1.91	0.039	-1.56	0.202
Syntaxin-binding protein 1	STXBP1	P61764	6.5	5.52	68	31	171	1.12	0.359	2.00	0.001	2.24	0.001
Tubulin alpha-1A chain (Fragment)	TUBA1A	F8VRZ4	5.44	5.09	12	22	67	-2.13	0.032	1.56	0.233	-1.37	0.299
Tubulin alpha-1B chain (Fragment)	TUBA1B	F8VVB9	5.03	5.54	28	46	91	-1.31	0.006	2.04	0.004	1.55	0.021
Tubulin alpha-1B chain (Fragment)	TUBA1B	F8VVB9	5.03	5.29	28	33	342	-1.26	0.377	-1.66	0.110	-2.09	0.020
Tubulin alpha-1B chain (Fragment)	TUBA1B	F8VVB9	5.03	5.23	28	33	128	-1.32	0.050	-2.97	0.041	-3.93	0.021
Tubulin beta-2A chain	TUBB2A	Q13885	4.78	5.45	50	34	139	1.19	0.490	-1.84	0.184	-1.55	0.421
Tubulin beta-4A chain	TUBB4A	P04350	4.78	4.81	50	16	62	-1.20	0.137	-1.84	0.004	-2.20	0.001
Tubulin beta-6 chain (Fragment)	TUBB6	K7ESM5	5.49	5.26	37	12	123	-1.59	0.298	-2.51	0.098	-4.01	0.036
Ubiquitin carboxyl-terminal hydrolase isozyme L1	UCHL1	D6R974	5.67	5.15	17	20	133	1.04	0.877	-2.47	0.022	-2.37	0.019

Table 2.2. Postsynaptic density proteins identified using MS/MS that have ±1.5 fold change in NDAN vs.AD.

Using this set of 31 proteins I then looked at AD vs. control and NDAN vs. control (Fig. 2.2) to determine if the changed protein would fall into any of the following categories:

1) progression of neuropathology – proteins that have more pronounced change in either AD, or NDAN when compared to control;
2) unique to AD – proteins that change in AD vs. control, but not in NDAN vs. control;
3) unique to NDAN – proteins that change in NDAN vs. control, but not in AD vs. control.

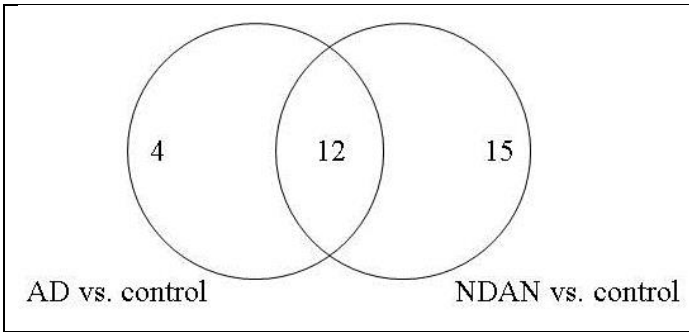

Figure 2.2. Venn diagram of the total number of proteins identified. Proteins with ±1.5 fold change in NDAN vs. AD are analyzed, including the number of proteins that change in AD vs. control and NDAN vs. control.

I also found several sets of protein spots on the 2DE with different isoelectric points and/or sizes that were identified as the same protein ("protein trains") (Table 2.3). The differences in theoretical and detected isoelectric points, with little to no change in sizes, could suggest post-translational modifications of the protein, while differences in protein size could indicate post-translational modifications and/or protein cleavage.

Protein	Theoretical pI	Theoretical Mw, kDa	Measured pI	Measured Mw	Fold change in NDAN vs. AD
Isoform 3 of dynamin-1, DNM1	6.57	96.04	4.88	19	-1.6
			4.93	20	1.96
Glial fibrillary acidic protein, GFAP	5.42	49.88	5	20	-4.32
			5.06	34	-2.07
			4.98	18	-1.98
			5.07	37	1.53
			5.18	46	2.06
			5.43	46	2.12
			5.28	46	2.15
			5.34	46	2.18
			5.39	46	2.58
Isoform 2 of glial fibrillary acidic protein, GFAP	5.53	50.28	5.74	48	-1.6
			5.16	49	1.53
			5.07	37	1.56
			5.5	46	1.6
			5.23	46	1.63
			5.17	38	1.63
			5.16	35	1.7
			5.09	36	2.42
Hemoglobin subunit beta, HBB	6.74	16	7.34	14	1.67
			7	14	1.84
			7.35	14	2.9
Keratin type I cytoskeletal 9, KRT9	5.14	62.06	4.82	13	-1.56
			6.14	17	1.55
Keratin type II cytoskeletal 1, KRT1	8.15	66.04	5.54	17	-3.1
			4.66	35	-1.81
			7.55	12	-1.54
Profilin-2, PFN2	9.26	9.84	5.06	13	-2.08
			5.76	14	-1.54
Isoform cytoplasmic + peroxiredoxin-5, mitochondrial	6.73	17	7.75	16	-2.27
Isoform 3 of peroxiredoxin-5, mitochondrial	9.12	17	7.7	15	-1.77
Isoform IB of synapsin-1, SYN1	9.88	70.03	8.87	74	-2
			9.17	75	-1.72
Tubulin alpha-1B chain, TUBA1B	5.03	27.55	5.23	33	-2.97
			5.29	33	-1.66
			5.54	46	2.04

Table 2.3. Proteins detected in trains of spots on the 2DE.

In the following discussion some of the proteins I have identified are usually found in the presynaptic terminals. It is important to note that the samples were prepared using a PSD-enrichment protocol, therefore, some of the presynaptic proteins were identified during the proteomic analysis. I elected to present these results as the presynaptic proteins contribute to the observed changes at the synaptic level.

Main upstream regulators

The thirty-one proteins were analyzed using Ingenuity Pathway Analysis (IPA) to determine main upstream regulators and pathways. Five upstream elements were identified as regulators of the changes that were observed: MAPT (microtubule-associated protein tau), PSEN1 (presenilin 1), APP (amyloid precursor protein), HTT (huntingtin) and D-glucose. MAPT, PSEN1, APP and HTT are known to play a role in Alzheimer's Disease pathogenesis ([15, 63, 64]; reviewed in [65-67]). Multiple studies with ^{18}F-fluorodeoxyglucose demonstrate that in AD there is a progressive reduction of glucose metabolism which correlates with severity of the disease (reviewed in [68]). Impaired glucose metabolism in the brain is one of the pathophysiological features that frequently precedes clinical manifestation in AD (reviewed in [68]).

Canonical pathways and molecular and cellular functions

IPA was used to identify pathways that the 31 changed proteins collectively represent or are a part of. The top canonical pathways returned by the IPA were: remodeling of epithelial

adherens junctions ($p = 5.14*10^{-12}$), epithelial adherens junction signaling ($p = 1.07*10^{-9}$), phagosome maturation ($p = 1.18*10^{-9}$), 14-3-3 mediated signaling ($p = 2.49*10^{-8}$), axonal guidance signaling ($p = 2.42*10^{-6}$), and gap junction signaling ($p = 3.75*10^{-6}$).

The molecular and cellular functions identified by IPA included cellular assembly and organization, cellular function and maintenance, and cell morphology. Interestingly, eleven proteins from our dataset cluster into the nervous system development and function pathway. This is consistent with our previous findings showing that when compared to AD and MCI, NDAN individuals have higher rate of neurogenesis in the dentate gyrus, which is positively correlated to their ability to escape (or significantly delay) dementia [40].

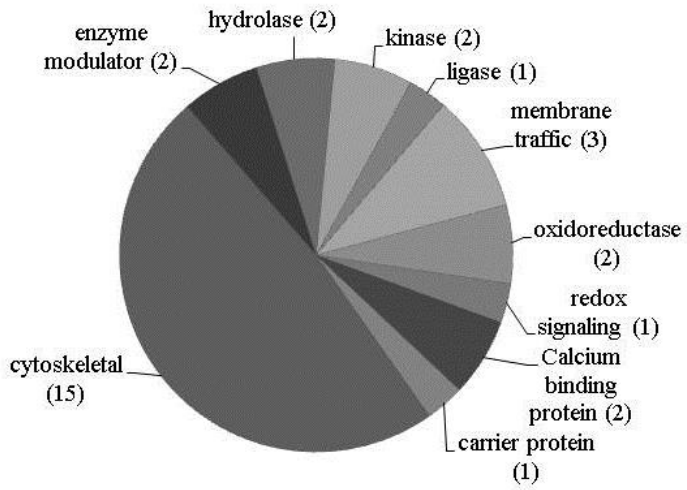

Figure 2.3. Pie chart representing the PANTHER classification of proteins based on protein class. The number of proteins in each category is shown in parenthesis.

PANTHER [69-71] was used to analyze relevant proteins by function (Fig. 2.3). Table 2.4 describes identified proteins in NDAN vs. AD by functional category.

Functional category	**Name of protein**	**Regulation in NDAN vs. AD**	**References**
Calcium binding proteins	Annexin 2	Up	[72-75]
	Calreticulin	Down	[76-86]
Carrier proteins	Hemoglobin	Up	[87-95]
Enzyme modulators	Ras-related protein Rap-1b	Up	[96-98]
	Rho GDP-dissociation inhibitor 1	Down	[99-101]
Hydrolases	2',3'-cyclin-nucleotide 3'-phosphodiesterase	Up	[102-104]
	Ubiquitin carboxyl-terminal hydrolase isozyme L1	Down	[105-110]
Kinases	Calcium/calmodulin-dependent protein kinase II subunit alpha	Up	[111-115]
	Creatine kinase B	Down	[116-120]
Ligases	Pyruvate carboxylase	Down	[121, 122]
Membrane traffic	Clathrin light chain A	Down	[123-125]
	Synapsin 1	Down	[126, 127]
	Syntaxin binding protein 1	Up	[128, 129]
Oxidoreductases	Glyceraldehyde-3-phosphate dehydrogenase	Up	[130-132]
	Malate dehydrogenase	Up	[133-136]
Redox signaling	Peroxiredoxin 5	Several isoforms identified	[137-141]
Cytoskeletal	Dynamin-1	Several isoforms identified	[142-145]
	Glial fibrillary acidic protein	Several isoforms identified	[146, 147]
	Keratin type I cytoskeletal 10	Several isoforms identified	[148]
	Keratin type I cytoskeletal 9	Several isoforms identified	[148-151]
	Keratin type II cytoskeletal 1	Several isoforms identified	[152, 153]
	Neurofilament medium polypeptide	Up	[154-156]
	Profilin-2	Down	[96, 157]
	Septin-7	Down	[158-160]
	Spectrin alpha chain	Down	[161-165]
	Tubulin alpha-1A	Up	[166]
	Tubulin alpha-1B	Several isoforms	[166]

		identified	
	Tubulin beta-2A	Down	[166]
	Tubulin beta-4A	Down	[166]
	Tubulin beta-6 chain	Down	[166]
	Vinculin	Up	[167, 168]

Table 2.4. PANTHER protein class analysis.

Discussion

Protein function and pathway analysis

The samples employed in this study consisted of PSD-enriched hippocampal fractions; the purity of PSD fractions prepared according to our protocol was previously described [39]. The proteomic methodology for this study was chosen for the superior quantitative aspects, but due to technical limitations of extraction and the 2DE methodology, hydrophobic or transmembrane proteins are not reliably represented in our dataset. Future studies focusing on transmembrane proteins will complement this initial work that therefore centers on soluble, non-transmembrane proteins. Among the 31 proteins that have significantly different levels in NDAN vs. AD, fifteen form a unique expression pattern in NDAN (Fig. 2.2), setting these individuals aside from both age-matched healthy controls and AD patients. Existence of the unique protein "signature" at the PSD of NDAN cases suggests that these non-demented subjects should not be considered pre-symptomatic AD, but rather individuals who are clearly distinct from both control and those who have clinical manifestation of the disease.

The unique protein expression signature in our dataset represents several pathways that converge onto junction signaling, phagosome maturation and 14-3-3 pathway. Additionally, twenty proteins from our dataset were clustered by IPA into the neurological disease pathway, which reveals that these proteins are closely related to each other and have been previously shown by other investigators to be implicated in brain diseases (Fig. 2.4). This latter observation corroborates the notion that relevant mechanisms may be acting at the NDAN synapses to mediate their resilience to neurodegeneration and associated dementia.

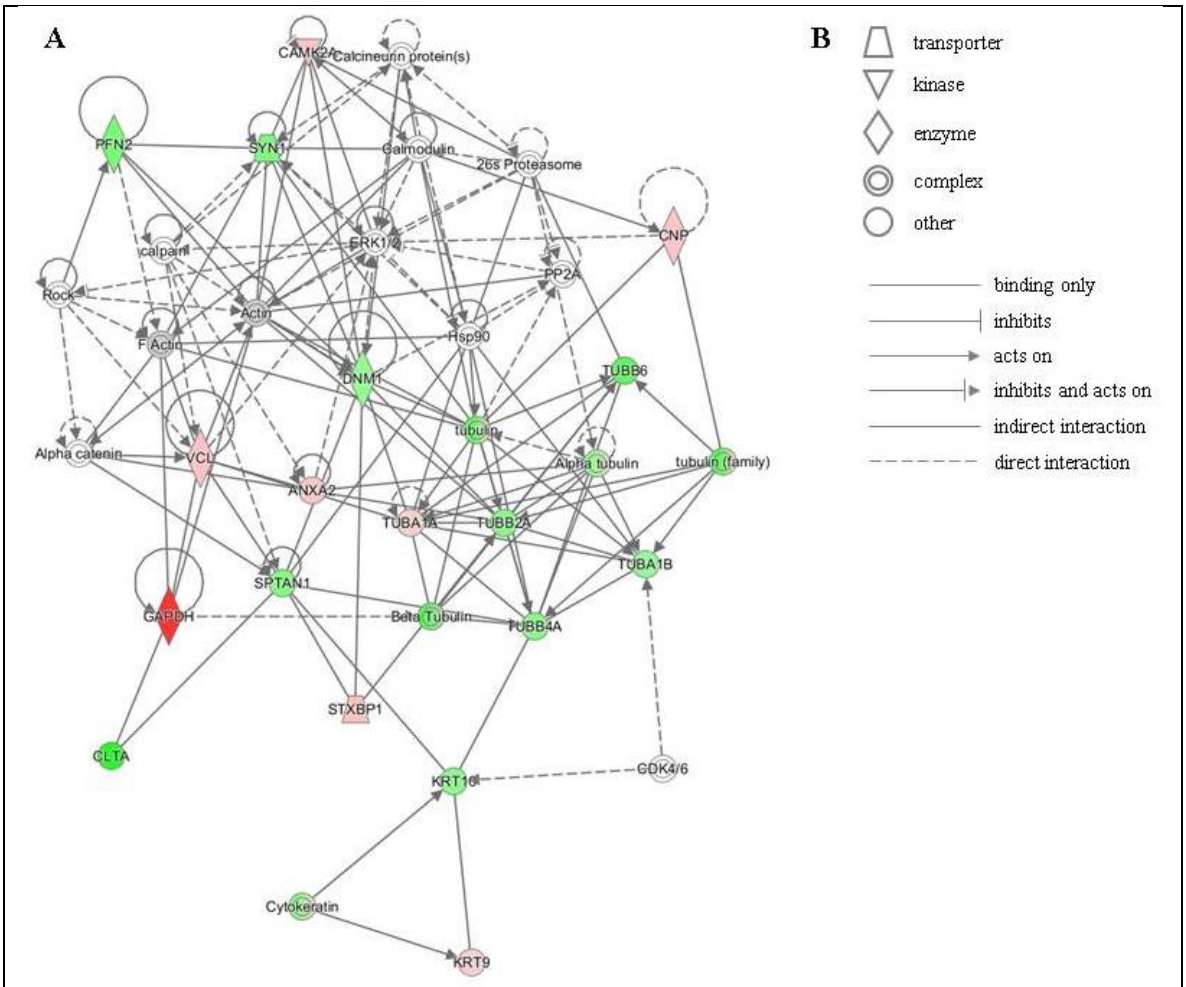

Figure 2.4. IPA identifies twenty proteins from our dataset that are associated with the neurological disease network. (A) Upregulated (red) or downregulated (green) proteins from our dataset are highlighted in the network. Solid and dashed lines indicate direct and indirect correlation between proteins, respectively. CAMK2A – calcium/calmodulin-dependent protein kinase type II subunit alpha; PFN2 – profilin-2; SYN1 – synapsin-1; CNP - 2',3'-cyclic-nucleotide 3'-phosphodiesterase; PP2A – protein phosphatase 2; ERK1/2 – mitogen-activated protein kinase 1/2; DNM1 – dynamin-1; Hsp90 – heat shock protein 90; TUBB6 – tubulin beta-6 chain; VCL – vinculin; ANXA2 – annexin 2; TUBA1A – tubulin alpha-1A chain; TUBB2A – tubulin beta-2A chain; TUBA1B – tubulin alpha-1B chain; TUBB4A – tubulin beta-4A chain; SPTAN1 – spectrin alpha chain, non-erythrocytic 1; GAPDH – glyceraldehyde-3-phosphate dehydrogenase; CLTA – clathrin light chain A; STXBP1 – syntaxin-binding protein 1; KRT10 – keratin, type I cytoskeletal 10; CDK4/6 – cyclin-dependent kinases 4/6; KRT9 – keratin, type I cytoskeletal 9. (B) Figure legend for the IPA network. Nodes in the network are depicted by different shapes that represent different functional class of the protein. Representation of molecular relationships in the IPA network.

Progression of neuropathology – proteins with a more pronounced change in either AD or NDAN

I found higher levels (1.83 fold) of annexin 2 (ANXA2) at the PSDs of NDAN subjects (1.55 AD vs. control, 2.85 NDAN vs. control). ANXA2 belongs to a group of soluble, hydrophilic proteins which can bind to negatively charged phospholipids in a Ca^{2+}-dependent manner [72]. ANXA2 has Ca^{2+}-dependent filament bundling activity and can participate in membrane vesicle aggregation, where it forms membrane-membrane or membrane-cytoskeleton connections by interacting with F-actin [72]. Notably, decreased levels of F-actin have been associated with synapse structural instability in AD (reviewed in [73]). ANXA2 has been demonstrated to modulate the activity of membrane channels, including Cl^- and Ca^{2+}; in addition, ANXA2 functions as a GLUT-4 transporter upon insulin stimulation [74]. Furthermore, ANXA2 interaction with tau modulates the tau mobility in the tips of neurites [75]. Therefore, higher levels of ANXA2 present in NDAN synapses could be indicative of preserved synaptic structure, function and insulin responsiveness.

Calcium/calmodulin-dependent protein kinase type II subunit alpha (CAMK2A) is a serine/threonine protein kinase and is required for hippocampal long-term potentiation (LTP) and spatial learning (as reviewed by [111]). Exposure to Aβ oligomers decreases the CAMK2 pool at the synapse [112]. CAMK2A-containing neurons are selectively lost in the CA1 of hippocampus in AD patients [113]. CAMK2 serves as a molecular switch for LTP and is capable of long-term memory storage [114]. CAMK2A levels are increased by 1.98 fold in NDAN when compared to AD (1.43 AD vs. control, 2.83 NDAN vs. control), which could indicate that robust CAMK2 upregulation is a necessary event to provide resistance of synapses to AD-related disruption as

seen in NDAN, an event that may occur to an insufficient extent in symptomatic AD. The functionality of CAMK2A is measured by the subcellular localization and phosphorylation at Thr286 [115], which were not assessed in this study. However, our previous study demonstrated that in AD the PSD immunoreactivity of the p(Thr286)CAMK2 is shifted away from the dendritic spines as it accumulates at the neuron's cell body in an Aβ oligomer-dependent phenomenon ([37], reviewed in [111]), and therefore, present results of CAMK2A levels at the PSD could reflect the compartmentalization of this protein.

Hemoglobin (HBB) was increased in NDAN vs. AD, a phenomenon consistently observed for each of the detected isoforms: 1.67 (1.75 AD vs. control, 2.92 NDAN vs. control), 1.84 (1.68 AD vs. control, 3.09 NDAN vs. control) and 2.9 fold (1.26 AD vs. control, 3.66 NDAN vs. control), which could suggest multiple scenarios. First, increased levels of HBB can indicate a response to hypoxia in brain. Indeed, decreased expression of hemoglobin in AD was observed in neurons containing NFTs [87]. Furthermore, nitric oxide and its metabolites have high affinity for HBB, and HBB can be considered a protectant from oxidative and nitrosative stress [88]. Besides nitric oxide scavenging, HBB is capable of binding Aβ and enhancing its aggregation ability due to the presence of the iron core; HBB was previously shown to localize to amyloid plaques in AD brains [89]. It is thus possible that in NDAN HBB is promoting Aβ removal from the synapses which is supportive of our previous findings [39]. On the other hand, HBB presence at the synapse could be due to leaky blood-brain barrier, which has been shown to occur in the aged and diseased CNS ([90, 91], reviewed in [92]). However, mRNAs for hemoglobin α- and β-chains were previously detected in rat and human neuronal cultures [93, 94], whereas human brain sections stained for HBB showed a granular pattern in the cytoplasm

without localization to specific compartments [94, 95], collectively suggesting a possible role of local HBB within neurons.

Malate dehydrogenase (MDH) is the terminal enzyme of the TCA cycle; its function is to catalyze the conversion of L-malate to oxaloacetate, which requires NAD as a cofactor [133]. In our dataset we found an increase in MDH2 at the PSD of 1.77 fold in NDAN as compared to AD patients (1.67 AD vs. control, 2.97 NDAN vs. control). While it has been reported that MDH levels can be elevated during caloric restriction in mice [134], a diet regimen known to reduce age-associated CNS deficits (reviewed in [135, 136]), the physiological significance of increased MDH at the synapses remains to be established [134].

Tubulin alpha-1A (-2.13 AD vs. control, -1.37 NDAN vs. control, 1.56 fold in NDAN vs. AD) and beta-6 (-1.59 AD vs. control, -4.01 NDAN vs. control, -2.51 fold in NDAN vs. AD) have significantly different abundance in NDAN vs. AD (Table 2.3). Tubulin alpha and beta are the main components of microtubules which are very dynamic structures. Microtubules undergo rapid growth and disassembly which could potentially explain the protein level variability in our dataset, as well as the possibility of multiple post-translational modifications (reviewed in [166]).

Interestingly, the majority of proteins in this category presented with higher fold change in NDAN vs. control, than in AD vs. control. It is therefore tempting to speculate that these proteins participate in the protective phenotype in NDAN, which is also observed in AD to a limited extent and is therefore possibly ineffective (and/or abortive).

Protein changes unique to AD

2',3'-cyclin-nucleotide 3'-phosphodiesterase (CNP) levels in AD were found to be -1.66 fold decreased vs. control. This finding is in agreement with previously published findings by Reinikainen *et al.* where they describe decreased CNP activity in hippocampus of AD patients [169]. Activity of CNP can be used as a measure of myelination of axons and lower levels of CNP in AD could be indicative of the loss of myelination of hippocampal neurons [102]. CNP hydrolyses 2',3'-cyclic nucleotides to create 2'-derivatives [103]. CNP can regulate tubulin polymerization and microtubule distribution [104], as microtubules use CNP as a linker, which allows them to connect to the plasma membrane. Additionally, CNP stimulates F-actin reorganization, which is essential for filopodia and lamellipodia formation [104]. CNP levels were unchanged in NDAN vs. control and were decreased in AD, which once again supports the idea that NDAN synapses remain healthy.

Glyceraldehyde-3-phosphate dehydrogenase (GAPDH) was found to be dramatically downregulated in AD vs. control (-6.19 fold). As reviewed by Butterfield *et al*., in addition to glycolytic activity, GAPDH performs many other functions: DNA and RNA binding, transcription regulation, kinase, catalysis of microtubule formation and polymerization, vesicular transport and interaction with multiple molecules and proteins, including NO, huntingtin and APP [130]. Additionally, GAPDH can undergo multiple post-translational modifications: oxidation, phosphorylation, S-nitrosylation, as well as direct or indirect interaction with oxidative species. GAPDH can interact with Aβ [131], and has been found to be a major component of amyloid plaques and NFTs in AD brains [130]. Aβ, on the other hand, was shown to stimulate inactivation of GAPDH in addition to promoting its nuclear translocation and pro-

apoptotic function [130]. GAPDH levels are decreased in AD which can indicate reduced glucose metabolism [132]. GAPDH has been suggested to be a potent target to prevent neurodegeneration in AD brains, due to ability of GAPDH to serve as scaffold for APP, Aβ40 and Aβ42, and tau protein [130, 131]. Levels of GAPDH in NDAN are unaltered when compared to control, which distinguishes NDAN from AD and can indicate better overall brain health of NDAN individuals.

Neurofilament medium polypeptide (NEFM) was measured at -1.28 in AD vs. control, which indicates a trend towards decrease in AD. Overall in NDAN vs. AD NEFM was changed by 1.5 fold (1.17 in NDAN vs. control). Neurofilaments play a role in establishing and maintenance of the 3D structure of axons [154]. NEFM is essential for the formation of the cross-bridge, stabilization, and extension of filament network [154, 155]. NEFM tail and its phosphorylation are required for radial growth of large myelinated motor axons [154]. Neurofilaments allow neurons to maintain their shape and are required for axon growth [156]. Neurofilaments can interact with microtubules, certain receptors that are located at the PSD and many other proteins that are transported along neurofilaments.

We found that the level of Septin-7 (SEPT7) was increased by 1.48 fold in the PSD of AD patients as compared to control subjects while remaining unchanged in NDAN vs. control. Septins are evolutionary conserved cytoskeletal GTPases. Septins can be found in NFTs, dystrophic neurites in senile plaques and neuropil threads in AD brains [158]. Some septin species are also found in granular or fine fibrillary deposits in neuronal soma [158]. Formation of septin fibrils suggests that aggregation of this protein may accompany NFT formation. In order to function properly, septins form filaments following a process regulated by GTP hydrolysis [158]. Dysregulation of normal septin assembly in neurons may result in affected vesicular

transport and structural integrity, leading to accelerated neurodegeneration. Interactions with phospholipids, microtubules and actin can influence septin assembly [160]. Septin assemblies can modulate the distribution of surface proteins and receptors and can also play a role in clathrin-mediated endocytosis [160]. It is thought that septins can serve as scaffolds for submembranous structures, assisting in neuronal polarity and vesicle trafficking [160]. SEPT7, in particular, can be located on the cytoplasmic side of presynaptic membranes and in endfeet of astroglia [159]. As reviewed by Mostowy and Cossart, SEPT7 plays a role in actin dynamics, axon growth, cell shape, chromosome segregation, cytokinesis, dendrite formation, DNA repair, membrane trafficking and microtubule regulation in addition to serving as a scaffolding protein [160].

Protein changes unique to NDAN

Calreticulin, a key upstream regulator of calcineurin [76], is a chaperone protein that can be found in several organelles in neurons and glial cells [77]. It is known to interact with APP, Aβ and Ca^{2+} [76, 78-82]. Calreticulin was found at lower levels (-3.27 fold) at the PSDs in NDAN when compared to control. While lower levels of calreticulin have been shown to be associated with decreased calcineurin activity [83, 84], increased calcineurin has been reported in the AD brain and correlates with disease severity [85, 86]. Furthermore, it was previously shown that calcineurin mediates the toxic action of Aβ oligomers at synapses and that pharmacological inhibition of calcineurin protects from AD-related memory deficits in both experimental animals and humans ([22, 170-172]; reviewed in [173]). Furthermore, we found that calcineurin levels are unaltered in the brain of NDAN subjects as compared to demented AD patients (Taglialatela

et al., unpublished observation). Therefore, reduced calreticulin levels at the synapses in NDAN individuals may be one of the mechanisms maintaining low calcineurin, thus contributing to preservation of synaptic integrity in the face of the presence of toxic amyloid oligomers.

Clathrin was downregulated in NDAN vs. control (-3.34 fold). Clathrin plays an important role in sorting and recycling of the proteins at the synaptic membrane [123]. While the protein levels of clathrin in AD are preserved when compared to control, the regulation of clathrin transport is known to be impaired in AD brains [123]. Under normal conditions clathrin is transported from neuronal perikarya to axonal terminals, with the highest concentration of clathrin found at the synaptic terminals [123]. However, Nakamura *et al.* report that in AD the amount of clathrin at synaptic terminals is decreased, while NFTs and neuronal perikarya have detectable levels of clathrin [123]. In the growth cones, repulsive Ca^{2+} signals cause asymmetric clathrin-mediated endocytosis via calcineurin [124]. Calcineurin activation results in clathrin- and dynamin-dependent endocytosis. Additionally, Aβ42 reduces axonal density by promotion of clathrin-mediated endocytosis in the growth cones, which results in a growth cone collapse due to Ca^{2+} signaling, and calcineurin and calpain activation [125]. Moreover, inhibition of clathrin-mediated endocytosis was demonstrated to rescue the Aβ42-induced toxicity [125]. Reduction of clathrin levels at PSD in NDAN in comparison to AD could thus be another contributing factor to the ability of NDAN synapses to withstand the toxic hit by Aβ which in AD results in increased endocytosis and growth cone retraction.

Creatine kinase B (CKB) levels were decreased at the PSDs of NDAN vs. control (-2.57 and -1.88 fold). The CKB family of enzymes is involved in the regulation of the ATP and ADP levels by reversible transfer of phosphate onto creatine to form phosphocreatine, which can provide energy when ATP concentrations drop [116, 117]. Additionally, CKB is identified as a

part of slow axonal transport [118]. CKB-deficient cells show significantly increased fraction of motile mitochondria [116]. While initial evidence suggests that synaptic mithochondria in NDAN have less DNA damage through a preserved mithocondrial DNA repair system (Taglialatela *et al.*, unpublished observation), we have not yet analyzed mitochondria function in NDAN vs. AD, nevertheless, it has been reported that mitochondria are severely impaired in AD [119, 120]. Interestingly, two subunits of the mitochondrial membrane respiratory chain Complex I were detected in our dataset. NADH dehydrogenase [ubiquinone] 1 alpha subcomplex subunit 5 (NDUFA5) and NADH dehydrogenase [ubiquinone] flavoprotein 1 (NDUFV1) did not meet the ±1.5 fold cut-off criteria in NDAN vs. AD, however, they were measured at -1.44 and -1.47 fold changes, respectively. Collectively these findings indicate the dysregulation of mitochondrial function in the presence of AD-like pathology. Mitochondria function and ATP generation in the brain can be affected by the improper glucose metabolism since Krebs cycle and oxidative phosphorylation of glucose occur in mitochondria (reviewed in [68]).

Activity of pyruvate carboxylase (PC) is tightly regulated. PC activity can be downregulated by insulin, which reduces the carbon flux when the glucose levels are high [121]. Lower levels of PC in NDAN (-1.59 fold vs. AD) could be explained by the fact that NDAN subjects, unlike AD, have preserved insulin responsiveness (Taglialatela *et al.*, unpublished observation). One of the important roles of PC pathway is detoxification of ammonia from the brain, during which glutamine synthetase catalyzes formation of glutamine from ammonia and glutamate. Conversion of pyruvate to oxaloacetate replenishes the TCA cycle, which is utilized during detoxification of ammonia or oxidation of glutamate [122].

Synapsin 1 (SYN1) is downregulated in NDAN vs. control (-1.71 and -1.48 fold). SYN1 is a member of a family of neuron-specific phosphoproteins that can be localized pre- and

postsynaptically [126, 127]. SYN1 plays a role in regulation of axonogenesis, synaptogenesis and regulation of nerve terminal function in mature synapses [126]. SYN1 is differentially distributed in different regions of the hippocampus. It is suggested that presynaptic SYN1 (approximately 60% of total SYN1) becomes associated with synaptic vesicles, while the postsynaptic 40% of this protein possibly represent the newly synthesized protein that will be transported to the nerve terminals [127].

Syntaxin binding protein 1 (STXBP1) is upregulated in NDAN vs. control (2.24 fold). STXBP1 is a syntaxin 1 binding protein [128]. Syntaxin 1 and STXBP1 form a complex at 1:1 ratio. STXBP1 can act as a chaperone for syntaxin [129]. Proteins of the STXBP1 family can interact with Rabs, small GTPases, and together they may play a role in vesicle trafficking and membrane fusion [129]. STXBP1 proteins can also contribute to specificity of membrane trafficking. It has been suggested that protein kinase C regulates the STXBP1-syntaxin interaction [129]. Syntaxin bound to STXBP1 cannot interact with other proteins, which indicates that STXBP1 can play a role in determining the binding partners for syntaxin and further complex formation [129]. Syntaxin was not detected in the current proteomics set, therefore, I cannot unequivocally conclude if the higher levels of STXBP1 correlate with those of syntaxin as part of the complex that these proteins are known to form.

Donovan *et al.* reported increased levels of ubiquitin carboxyl-terminal hydrolase isozyme L1 (UCHL1) in AD when compared to healthy individuals [105]; we found a decrease in UCHL1 levels at the PSD in NDAN (-2.37 NDAN vs. control). UCHL1 can associate with free ubiquitin in neurons, which suggests that this interaction is important for maintenance of the free ubiquitin pool in neuronal cells [106, 107]. UCHL1 is expressed mostly by neurons and neuroendocrine cells, and it was found in Lewy bodies [108] and NFTs [109]. Interestingly,

Lombardino *et al.* showed that replaceable neurons have lower levels of UCHL1 when compared to non-replaceable neurons [110], which can be in concordance with the increased neurogenesis in NDAN [40] – one of the hypothesis behind NDAN preserved cognitive function.

Several proteins involved in actin dynamics were uniquely affected in NDAN. Actin and other cytoskeletal proteins are responsible for changes in spine morphology. Dendritic spine dynamics are determined by actin cytoskeleton organization [96]. Ability of spines to change their structure allows for synaptic plasticity and plays an important role in memory formation [96]. Therefore, it is not unreasonable to argue that the changes in this class of proteins described below and uniquely observed in NDAN subjects are intimately associated with their preservation of synaptic integrity and cognitive ability ([39, 41, 42, 46, 173], reviewed in [53]). Cytoplasmic actin 2 showed a trend for downregulation in NDAN when compared to AD (-1.49). Actin is responsible for stabilization of synaptic boutons in addition to modulation of bouton's structure to adjust to postsynaptic signaling [96]. The interaction between actin and profilins is essential for proper actin polymerization [157]. Profilins provide actin monomers to the barbed-end polymerization of actin filaments [96]. Profilin 2 was found to be downregulated in NDAN when compared to control by -2.06 fold. Furthermore, vinculin (VCL) was upregulated in NDAN vs. control by 1.97 fold. VCL plays an important role in focal adhesion strengthening and stabilization due to its interaction with actin and talin [167]. At the leading edge of focal adhesion, VCL coordinates actin organization and dynamics. VCL determines the architecture of the leading edge by engaging actin flow to the extracellular matrix at maturing focal adhesion [167]. Vinculin binds to actin directly; however, vinculin also has an effect on actin dynamics independent of direct binding [167, 168]. Interestingly, stabilization and maturation of focal

adhesion are two distinct processes, as VCL inhibits the maturation of focal adhesion, but stimulates the stabilization [167].

Keratin type I cytoskeletal 10 (KRT10) is downregulated in NDAN vs. control by -1.87. Changes in KRT10 in tear proteome were reported by Kalló *et al.* in AD patients [148]. Keratins are normally abundant in epidermal tissue, however, several other research groups have identified keratin 1 and 9 in samples of blood and CSF (keratin 1 and 9 are discussed in *Protein isoforms*).

Significant decreases in tubulin beta-2A and 4A were observed in NDAN vs. control (-1.55 and -2.2, respectively). As discussed above, tubulin is a major component of microtubules and is a very dynamic protein.

NDAN PSDs have higher levels of Ras-related protein Rap-1b (1.62 in NDAN vs. control). Rap1B, a small GTP-binding protein [174], in growth cones of hippocampal neurons is required for axonal development and growth [97]. Rap1B works together with Cdc42, whereas Rho and Rac function as antagonists to regulate extension of axons and neurites [96]. Cdc42 is a member of Rho GTPase family that plays a role in differentiation of oligodendrocytes, axon outgrowth, and neuronal polarity and migration (reviewed in [98]). Rap1B is reported to regulate plasma membrane Ca^{2+} transport, enhancing protein kinase C activity which is needed at the tip of axon [97]. Consequently, Rap1B possibly functions as a positioning factor for protein kinase C [97] and increased Rap-1b at NDAN synapses could support the notion that NDAN synapses retain proper function.

Another molecule, Rho GDP-dissociation inhibitor 1 (RhoGDI), from the same pathway was downregulated in our dataset (-1.5 fold in NDAN vs. control). Levels of RhoGDI are typically in balance and roughly equivalent to combined levels of RhoA, Rac1 and Cdc42 [99].

RhoGDI functions as stabilizer for Rho proteins, protecting them from degradation [99]. Due to the complex regulation of RhoA/Rac1 cell signaling and the fact that RhoA, Rac1, or Cdc42 were not detected in the PSD fractions – the exact meaning of altered RhoGDI levels in the NDAN PSD remains unclear. On the other hand, Cdc42/RhoA/Rac1 network is involved in actin assembly/disassembly in response to extracellular stimuli [100, 101] and data reported here indicate that this signaling pathway regulation differs in NDAN vs. AD as can be inferred by the levels of some key players of this network, including RhoGDI and Rac1.

As reviewed by Yan and Jeromin, remodeling and degradation and overall metabolism of spectrin (SPTAN1) play a role in the maintenance of membranes and cytoskeleton, protein cleavage, recycling and degradation [161]. SPTAN1 was downregulated in NDAN vs. control (-1.56 fold). Interactions between spectrin and other membrane-anchored proteins allow for proper trafficking and dynamics of proteins within the lipid bilayer. In the brain, SPTAN1 is estimated to comprise approximately 3% of total membrane protein content, being present in neuronal cell bodies, dendrites and postsynaptic terminals [161]. Additionally, SPTAN1 can localize to plasma membrane, microtubules, mitochondria, endoplasmic reticulum and nuclear envelope. In AD, SPTAN1 and its breakdown products are increased and have been proposed to be used as a biomarkers in AD patients [161-163]. At the PSD, spectrin functions as a connector between integral membrane proteins and actin (reviewed in [164]). SPTAN1/synaptosomal membrane interaction is inhibited by Ca^{2+}/calmodulin [165]. Spectrin interaction with NMDAR mediates the regulation of NMDAR activity, which can be the basis for plasticity-induced changes in spines (reviewed in [164]).

Multiple cytoskeletal proteins as well as their regulators are altered in NDAN vs. AD, which could indicate active remodeling of the synapses. These findings concur with the

observations reported by others regarding preserved synaptic integrity in NDAN [3, 52, 54, 175]. Collectively these results suggest that the complex regulation of structural proteins in NDAN contributes to Aβ resistance.

Protein isoforms

Dynamin-1 (DNM1) is a large neuron-specific GTPase that is present at presynaptic terminals, where it is involved in synaptic vesicle budding off the membrane and recycling for future release [142]. DNM1 expression is dependent on CREB1 level [143]. DNM1 plays a role in formation of associative memory in hippocampus [144]. Dynamin in complex with other presynaptic proteins (*e.g.*, synapthophysin) participates in plasticity by modulating the efficiency of vesicle release. When DNM1 was knocked down in AD animal models, Aβ levels were lowered possibly due to regulation of BACE1 internalization [145]. Conversely, in tissue culture (hippocampal neurons) application of Aβ causes the decrease of DNM1 levels via calpain-mediated proteolysis [142]. Interestingly, this reduction of DNM1 occurs prior to synapse loss in cultured hippocampal neurons, which suggests the intriguing hypothesis that synapses become dysfunctional first and later the synapse retraction/loss occurs. In the dataset presented here two protein spots for DNM1 were identified on 2DE with fold change of 1.69 and -1.6 in NDAN vs. AD. It remains to be established if the DNM1 undergoes a post-translational modification which could explain different levels of this protein in our dataset.

Several isoforms of glial fibrillary acidic protein (GFAP) were detected, which can be expressed by several cell types in the brain, including neurons [146]. In concordance with other published studies [147], several horizontal “trains” of GFAP on the 2DE were identified in our

study (18 spots on the gel) (Table 2.3), which could indicate protein cleavage and/or degradation, co-translational or post-translational modifications that can affect the structure and function of GFAP. GFAP can undergo many post-translational modifications, such as phosphorylation, sulfation, glycosylation, oxidation, acetylation and other [176]. Each modification can result in different alteration of GFAP function and/or localization, although the exact mechanisms are still under investigation.

Keratin type I cytoskeletal 9 (1.55 and -1.56 fold in NDAN vs. AD) and keratin type II cytoskeletal 1 (-3.1, -1.54 and -1.81 fold in NDAN vs. AD) are expressed at significantly different levels in NDAN vs. AD (Table 2.3). Notably, keratin 9 was identified by multiple research groups in the CSF and has been even proposed as a biomarker for AD [149-151]. Furthermore, keratin 1 was identified in 5xFAD mouse hippocampi using proteomics [152], and keratin 1 and 9 show different expression patterns in other neurodegenerative disorders [153].

Several isoforms of tubulin alpha-1B with fold change of 2.04, -1.66, and -2.97 were significantly different between NDAN and AD. The possible significance of tubulins in the maintenance of synaptic function/stability in NDAN vs. AD has been discussed earlier.

Peroxiredoxins (PRDX) play a role in protection from oxidative stress, cell differentiation, proliferation, immune response and apoptosis [137]. Lower levels of PRDX5 (-1.77 and -2.27 fold) were found at the PSD of NDAN vs. AD, which can potentially indicate decreased oxidative stress in the brains of these individuals [138]. PRDX5 can neutralize hydrogen peroxide, alkyl hydroperoxides and peroxynitrite [139, 140] and its expression is increased during oxidative stress [141]. Peroxynitrite can alter the mitochondrial electron transport chain, therefore, efficient neutralization of peroxynitrite can be neuroprotective [141].

CHAPTER 3. Upstream Regulators of the Synaptic Proteome Changes

Background

Unveiling the yet unclear mechanisms responsible for preservation of cognitive function in NDAN is important as it would support a new treatment strategy centered on inducing cognitive resistance in anyone affected by AD. Unlike AD patients, NDAN show little to no synapse loss [54]. It was previously reported that the post-synaptic density (PSD) of NDAN subjects is resistant to Aβ oligomer binding [39], therefore protecting synapses and likely contributing to maintenance of cognitive ability despite the presence of AD neuropathology. During the analysis of the postsynaptic proteome of hippocampi of control (non-demented, age-matched), AD and NDAN using the IPA (Ingenuity Pathway Analysis) Upstream Regulators tool I discovered several intriguing upstream regulators. This tool can identify the upstream regulators which could explain observed changes in protein levels at the PSDs described in Chapter 2. Activation z-score describes the activation state of predicted regulator. Using the ±1.5 z-score cut-off for the upstream regulators, five miRNAs were identified as major drivers for the changes observed at the PSD of NDAN subjects.

miRNA

MicroRNAs (miRNAs) are 18-22 nucleotide long single-stranded RNAs that have mRNA complementary region. Each miRNA can target multiple messenger RNAs (mRNAs) via Watson-Crick base pairing. miRNAs are involved in multiple processes and their expression is regulated by enzymes which process and stabilize mature miRNA or by epigenetic mechanisms

such as DNA methylation or histone modifications [177]. MiRNAs are essential for organism development and are found to be dysregulated in several diseases, including AD [178-181]. MiRNA profile changes with age [182]. It is hypothesized that in neurodegenerative diseases miRNAs can modulate the levels of toxic proteins by regulating the mRNA encoding the toxic protein itself or by regulating the mRNA levels of proteins that regulate the levels of toxic proteins [183].

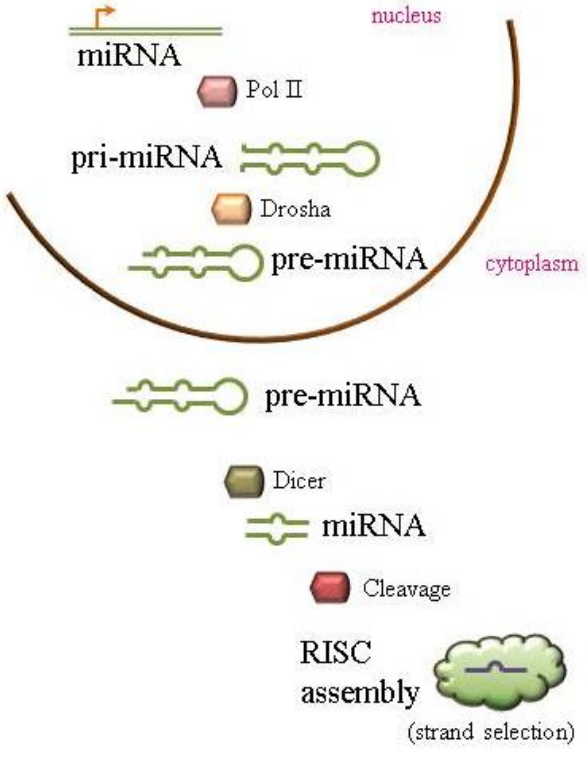

Figure 3.1. MiRNA processing in the cell. Pol II – RNA polymerase II, RISC – RNA-induced silencing complex. Modified from [184].

As schematically depicted in Fig. 3.1, miRNA transcription by RNA polymerase II occurs in the nucleus with the first step being the production of precursor primary miRNA (pri-miRNA). Pri-miRNAs are further processed in the nucleus where Drosha associates with other

factors to yield hairpin-shaped premature miRNA (pre-miRNA) that will be next processed in the cytoplasm. Once in cytoplasm, pre-miRNA becomes mature miRNA after cleavage by Dicer. Mature miRNAs can associate with RNA-induced silencing complex (RISC). RISC facilitates and stabilizes interactions between mRNA and miRNA. In neurons, there is evidence that Dicer and other miRNA processing machinery are expressed in dendritic spines to allow for local regulation of mRNA levels [185]. Dicer can be stimulated by synaptic activity, which leads to local processing of miRNA allowing for precise regulation of mRNAs at active synapses [185].

Mature miRNA can bind to miRNA recognition elements or 3'UTR of mRNA and induce mRNA degradation or block its transcription (Fig. 3.2). MiRNA action can result in small changes (less than 50%) in mRNA levels or completely switch the genes on or off [184].

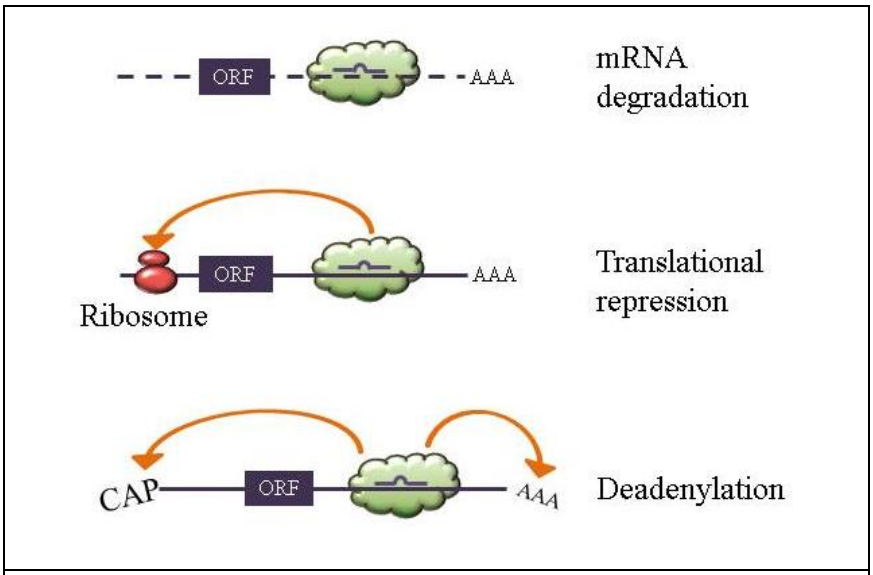

Figure 3.2. MiRNA binds to mRNA to initiate mRNA degradation. ORF – open reading frame, CAP – 5' cap, AAA – poly A tail. Modified from [184].

Based on the observations described in Chapter 2 and the IPA prediction of differential miRNA expression, we hypothesized that global action of miRNAs allows NDAN synapses to

acquire resistance to Aβ oligomer binding and toxicity. In this chapter I describe three miRNAs that are expressed at different levels in control, AD and NDAN. Manipulating the levels of these specific miRNAs and their effect on Aβ oligomer association with the synapses is described.

Methods

RNA isolation and real-time PCR

Following the manufacturer's protocol, RNA was isolated using Trizol Reagent (Life technologies, Carlsbad, CA, USA) from post-mortem frozen human frontal cortices of control, AD and NDAN (n=4). Approximately 100 mg of tissue was placed in Trizol and homogenized using the Polytron homogenizer (ThermoFisher Scientific, Waltham, MA, USA). Chloroform was then added and the samples were spun down at 12,000 rpm for 15 min at 4ºC. The aqueous phase was transferred to a new tube containing isopropanol. The samples were centrifuged at 12,000 rpm for 10 min at 4ºC. Pellet was washed with ice cold 80% ethanol and air-dried. The samples were resuspended in 40 µl nuclease free water. The RNA concentration was measured using NanoDrop 2000c (ThermoFisher Scientific, Waltham, MA, USA).

miRNA qPCR: Reverse transcription was performed using miScript II RT Kit (Qiagen, Hilden, Germany) according to manufacturer's protocol. Briefly, 0.5 µg RNA was reverse-transcribed in 20 µl reaction volume containing 4 µl 5x HiSpec buffer, 2 µl 10x miScript Nucleics mix and 2 µl miScript Reverse transcriptase. The mix was incubated at 37ºC for 1 hr, then at 95ºC for 5 min and placed on ice. The reverse transcribed miRNA mix was diluted with nuclease free water to final concentration of 3 ng/µl. Real-time PCR was performed to quantitate miRNA in control, AD and NDAN. miScript SYBR Green PCR Kit (Qiagen, Hilden, Germany) was used according to manufacturer's protocol. Briefly, the reaction was performed in 25 µl final volume in each well containing 3 ng reverse transcribed miRNA, 1x SYBR Green, reverse and forward primers (Qiagen, Hilden, Germany). The reaction was performed in Mastercycler

epgradient S (Eppendorf, Hamburg, Germany). The samples were incubated at 95ºC for 15 min to activate the polymerase followed by 40 cycles of amplification: 94ºC for 15 sec, 55ºC for 30 sec and 70ºC for 30 sec. Standard melting curve was performed at the end. The levels of miRNAs were normalized to U6 snRNA. The relative fold change in expression of target miRNAs was determined using the comparative cycle threshold method ($2^{-\Delta\Delta Ct}$).

mRNA qPCR: cDNA was made using amfiRivert Platinum cDNA Synthesis Master Mix (GenDEPOT, Katy, TX, USA) according to manufacturer's protocol. Online databases (miRBase.org, microRNA.org, mirdb.org) were used to select mRNA targets for each miRNA [186-190]. The primer sequences were obtained from the PrimerBank (https://pga.mgh.harvard.edu/primerbank/, Harvard, Cambridge, MA, USA) to measure expression of target genes. Quantitative real-time PCR (qRT-PCR) was performed to measure mRNA levels of selected genes. Each well of 96-well plate for qRT-PCR contained 20 ng RNA, 1 mM oligo and 1x KAPA SYBR FAST Universal qPCR kit (KAPA Biosystems, St. Louis, MO, USA). All samples were run in duplicate and normalized to actin. Standard melting curve was performed at the end. The relative fold change in expression of target miRNAs was determined using the comparative cycle threshold method ($2^{-\Delta\Delta Ct}$).

Aβ oligomer preparation

Aβ oligomers preparation is a technique, used routinely by our laboratory [39]. Briefly, lyophilized Aβ aliquots (Department of Biophysics and Biochemistry, Yale University, New Haven, CT, USA) were dissolved in 200 µl of 1,1,1,3,3,3-hexafluoro-2-propanol and then added to 700 µl of distilled deionized H_2O in microcentrifuge tubes. Loosely capped tubes were stirred

on a magnetic stirrer in a fume hood for 48 hours and then aliquoted and stored at -80ºC. In order to prepare labeled Aβ oligomers, a small aliquot of HiLyteTM Fluor 647-labeled Aβ1-42 (AnaSpec) was added at the beginning of Aβ oligomer preparation protocol.

Cell culture and transfection

SH-SY5Y cells (ATCC) were cultured in Eagle's minimum essential medium with non-essential acids and Ham's F12 medium and 10% FBS at 5%CO_2. The day before transfection the cells were plated in a 6-well plate at 20,000 cells/well. MiRNA mimics and inhibitors as well as negative control (ThermoFisher Scientific, Waltham, MA, USA) were dissolved in nuclease-free water to a final concentration of 50 µM. The transfection was performed using Lipofectamine2000 (ThermoFisher Scientific, Waltham, MA, USA) according to manufacturer's protocol. Briefly, in separate tubes, the miRNAs and Lipofectamine2000 were diluted in serum-free/antibiotic-free medium and incubated at room temperature for 5 min. Diluted Lipofectamine2000 was added to each tube containing miRNA drop-wise, inverted several times and incubated for 20 min at room temperature to allow for complex formation. Each well received 50 nM of miRNA. The growth media was replaced 24 hours post-transfection. The cells were collected 48 hrs post-transfection. Each well also received control siRNA tagged with FAM (ThermoFisher Scientific, Waltham, MA, USA) to control for transfection efficiency.

Flow cytometry

The SH-SY5Y cells were lifted with 10 mM EDTA, spun down and resuspended in 3% BSA in PBS. In order to measure the Aβ association with the cellular surface, the cells were incubated with several concentrations of Aβ oligomers (0.05-7 μM) for 30 min at room temperature. The cells were washed in 3% BSA in PBS by centrifugation at 1,250 x g for 5 min at 4ºC. The pellet was resuspended in 4% PF in PBS and incubated at room temperature for 10 min. The samples were then washed in PBS and resuspended in PBS without Ca^{2+}/Mg^{2+} and analyzed using Guava easyCyte flow cytometer (Merck Millipore, Burlington, MA, USA). In order to assess the Aβ oligomer interaction with cellular surface those cells manifesting green fluorescence (siRNA-FAM) and binding Aβ oligomers (red fluorescence) were analyzed.

Animals

Eleven to thirteen weeks old wild-type female C57B6 mice were purchased from the Jackson Laboratory (Bar Harbor, ME, USA). Health care for all animals was provided by the animal care specialists under a supervision of the facilities manager. The daily care and maintenance was provided for the animal colony on daily bases to ensure the safe and healthy environment. Each animal was used under an animal protocol approved by IACUC, ensuring that the animals receive the minimal amount of pain/discomfort. Every effort is made to minimize discomfort of animals while undergoing ICV injections. Since the brain has no pain receptors, the only discomfort the animal would experience would be pain at the needle injection site. The animal would experience neither locomotor impairment, nor the impairment of eating and

drinking. The animals were monitored immediately following the ICV injections until recovered from anesthesia by the experimenter.

For euthanasia, mice were deeply anesthetized with CO_2 until they were unresponsive. Cervical dislocation followed by decapitation was performed.

ICV injections

Wild-type female mice were injected intracerebroventricularly (ICV) with miRNA mimics or inhibitors (ThermoFisher Scientific, Waltham, MA, USA) dissolved in artificial cerebrospinal fluid. Hsa-let-7c inhibitor and miRNA-1 mimic (ThermoFisher Scientific, Waltham, MA, USA) were used as positive controls; one animal per dose was used. Seven animals per group were used for the ICV injections of miRNA-149, -4723, -485 mimics and inhibitors and scrambled miRNA (ThermoFisher Scientific, Waltham, MA, USA).

ICV injection is a technique routinely used by our laboratory [22]. Briefly, mice were anesthetized with isoflurane. The ICV injections were performed according to the freehand injection method described by Clark *et al.* [191]. 29-gauge needle was held with hemostatic forceps to leave 4 mm of the needle tip exposed. The needle was connected to a 25 µl Hamilton syringe via 0.38 mm polyethylene tubing. The injection volume varied based on the experiment and desired amount of miRNA to be delivered; infusion rate was set at 1 µl/min using electronic programmable microinfuser (Harvard Apparatus, Cambridge, MA, USA). After the injection, the needle was left in place for 1 min. The mouse was allowed to recover while lying on a heated pad under warm light. Twenty-four hours post-injection mice were euthanized by using deep

anesthesia followed by cervical dislocation. Mouse brain was quickly collected and stored at -80ºC for further analysis.

Results

Upstream regulators of changes in NDAN PSD proteome

The postsynaptic proteome dataset described in Chapter 2 was used to determine the upstream regulators of the changes observed. Unique protein signatures of control, AD and NDAN individuals were analyzed using IPA (Ingenuity Pathway Analysis) Upstream Regulators tool. This tool can identify the upstream regulators which could explain observed changes in protein levels. Activation z-score describes the activation state of predicted regulator. Using the ±1.5 z-score cut-off for the upstream regulators, five miRNAs were identified as major drivers for the changes observed at the PSD of NDAN subjects:

- miRNA-4723 (z-score = 2.607);
- miRNA-3180 (z-score = 2.2);
- miRNA-149 (z-score = 2.169);
- miRNA-4667 (z-score = 1.698);
- miRNA-485 (z-score = 1.561).

A literature search revealed that miRNAs-4723, -149 and -485 are involved in regulation of synaptic genes, whereas increased levels of miRNA-3180 were found in colorectal cancer [192], the function of miRNA-4667 is currently unknown. We have decided to focus on three miRNAs (4723, 149 and 485) due to their potential involvement in synaptic health and AD (Fig. 3.3).

MiRNA-149 (Fig. 3.3A) regulates Specificity protein 1 (Sp1) [193], APP, BACE1, tau, HDAC1/2, huntingtin and DNMT1 [194]. MiRNA-485 (Fig. 3.3B) regulates the expression of

BACE1, tau, dendritic spine density and number, PSD95 clustering, surface GluR2, and the miniature excitatory postsynaptic currents frequency [195-197]. MiRNA-4723 (Fig. 3.3C) regulates c-Abl [198], which can also be regulated directly by Aβ oligomers [199]; c-Abl can regulate the expression of synaptic genes via HDAC2 [200].

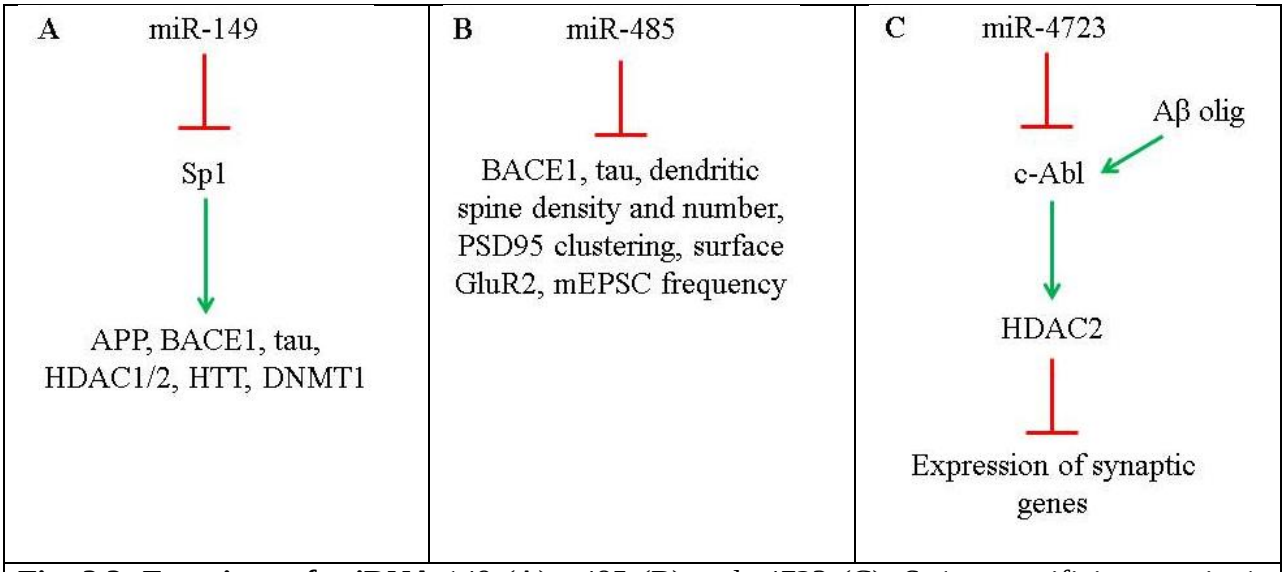

Fig. 3.3. Functions of miRNA-149 (A), -485 (B) and -4723 (C). Sp1 – specificity protein 1, APP – amyloid precursor protein, BACE1 – beta-secretase 1, HDAC1/2 – histone deacetylase ½, HTT – huntingtin, DNMT1 – DNA methyltransferase, PSD95 – postsynaptic density protein 95, GluR2 – glutamate receptor 2, mEPSC – miniature excitatory postsynaptic currents, c-Abl - Abelson tyrosine-protein kinase 1.

I have experimentally determined the levels of selected miRNAs in post-mortem human brains and found that they are indeed, as predicted by IPA, differentially regulated in AD and NDAN when compared to control. Changes in miRNA-4723 (Fig. 3) did not reach significance, however, a trend towards decrease in both AD and NDAN was observed. MiRNA-149 (Fig. 3) was significantly decreased in AD and NDAN when compared to control. MiRNA-485 (Fig. 3) was significantly downregulated in AD and showed a strong trend for downregulation in NDAN when compared to control.

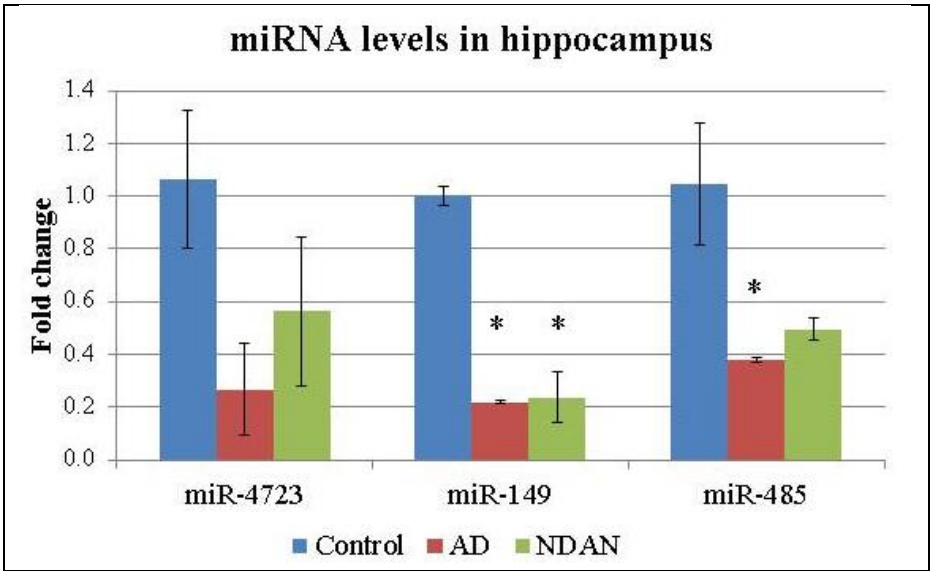

Figure 3.4. MiRNA levels in hippocampus of control, AD and NDAN. When compared to control miRNA-4723 levels are decreased in AD and NDAN, however, do not reach significance. miRNA-149 and miRNA-485 are downregulated in AD and NDAN when compared to control. n=4. * - $p<0.05$ vs control, t-test.

MiRNA levels in SH-SY5Y

SH-SY5Y neuroblastoma cell line was used to study the effect of modulation of miRNA levels on Aβ oligomer association with the cellular surface.

In order to determine the optimal concentration of miRNA for transfection, SY5Y cells were treated with 10 and 50 nM scrambled FAM-tagged siRNA. 10 nM siRNA resulted in 32% transfection efficiency, with 50 nM siRNA resulting in 63% transfected cells (Fig. 3.5A). 50 nM miRNA was selected for all further studies due to better transfection efficiency.

Next, I optimized the concentration of Aβ oligomers to be used for detection of Aβ oligomer association with the cellular surface. SH-SY5Y cells were detached using EDTA in order to preserve cell surface receptors, and then incubated with various concentrations of Alexa-

647 labeled Aβ oligomers (Fig. 3.5B). After testing several concentrations, 2 μM of Aβ oligomers was chosen for all further experiments.

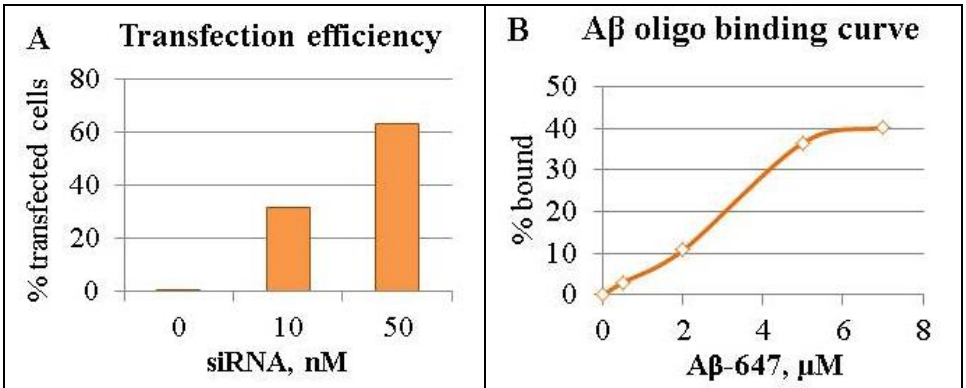

Figure 3.5. SY5Y transfection optimization. (A) SY5Y cells transfected with 10 and 50 nM FAM-tagged siRNA. Transfection efficiency was measured using flow cytometry. (B) SY5Y cells were lifted with EDTA and incubated with Alexa-647 labeled Aβ oligomers prepared in the lab. Cells were incubated with Aβ oligomers for 30 min at room temperature; the Aβ binding was evaluated using flow cytometry.

Next, to determine if the miRNA levels are altered by Aβ oligomers, the levels of endogenous miRNAs were measured in SH-SY5Y cells treated with 1μM Aβ oligomers overnight. As can be seen in Figure 3.6 levels of miRNA-4723 dropped below detection limit after treatment with Aβ oligomers; miRNA-485 was inhibited by 80% after treatment with Aβ; miRNA-149 was slightly downregulated. I have decided to focus on miRNA-485 and -4723 for further experiments.

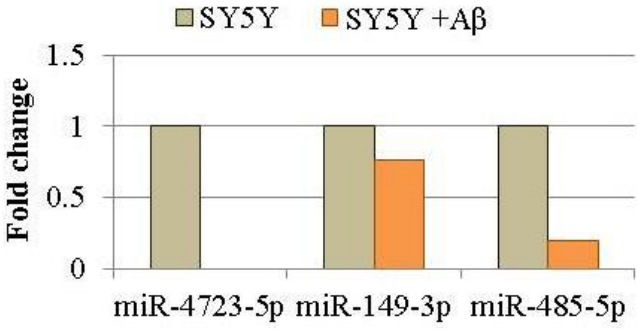

Figure 3.6. Overnight treatment with 1 µM Aβ oligomers downregulates selected miRNAs. All three miRNAs are altered after Aβ oligomer application.

Modulation of miRNA levels in SH-SY5Y

To determine if the amount of miRNA delivered to cells is sufficient to inhibit target mRNAs, I have identified target mRNAs for each miRNA. Target mRNAs were measured in SY5Y 48 hours post-transfection using qPCR.

MiRNA targets were selected using freely available online databases: www.mirdb.org and www.targetscan.org. PPP1R9B, protein phosphatase 1, was selected as a target of miRNA-4723-5p. STX5, syntaxin 5, is a target of miRNA-485-5p. As shown in Figure 3.7, PPP1R9B, a target gene of miRNA-4723, was downregulated when SH-SY5Y cells were transfected with the miRNA-4723 mimic, and upregulated after transfection with the inhibitor. Levels of STX5, targeted by miRNA-485, were regulated by the miRNA-485 mimic and inhibitor in a similar fashion (Fig. 3.7). MiRNA-4723 and -485 did not regulate their non-target mRNAs, STX5 and PPP1R9B, respectively.

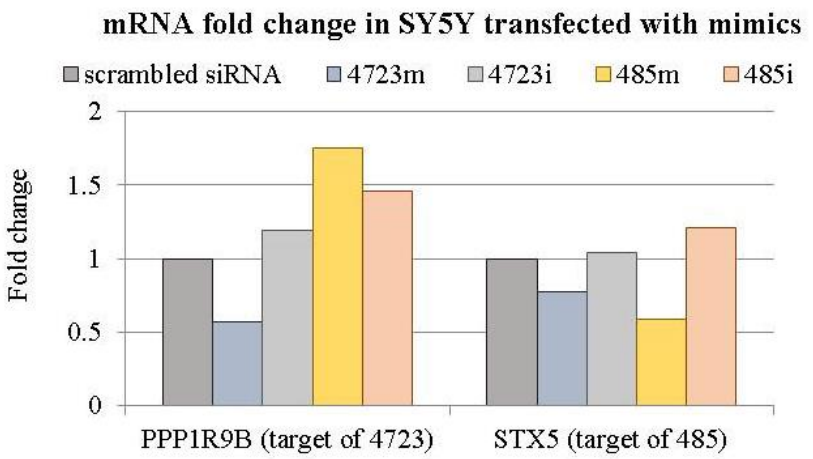

Figure 3.7. Target gene expression levels in SY5Y following transfection with mimics and inhibitors. PPP1R9B and STX5 levels were altered in response to transfection with miRNA mimics or inhibitors (mRNA inhibited with mimic and upregulated with inhibitor). PPP1R9B - Protein phosphatase 1 regulatory subunit 9B, STX5 – syntaxin 5.

Next, the Aβ oligomer association with the surface of SH-SY5Y was measured using flow cytometry (Fig. 3.8). To determine the effect of miRNA-4723 and -485 up- or downregulation on the Aβ oligomer association with the cell surface, 48 hours post-transfection SH-SY5Y cells were collected for flow cytometry analysis.

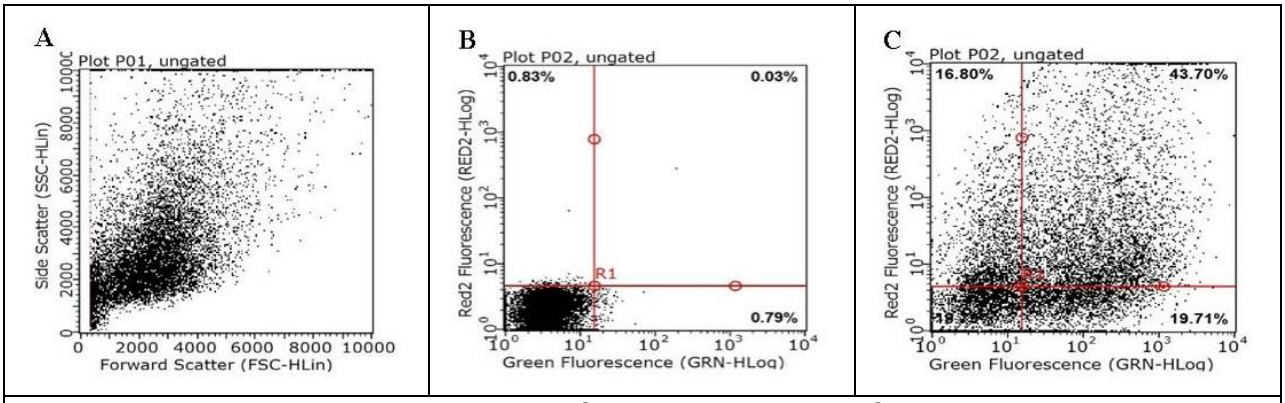

Figure 3.8. Representative acquisition of SY5Y cells during flow cytometry analysis. (A) SY5Y cells are gated according to their size. (B) Non-transfected cells without Aβ oligomers are used to set up quadrants for analysis. (C) SY5Y transfected with FAM-labeled scrambled siRNA (green fluorescence) and incubated with 5 μM Alexa-647 labeled Aβ oligomers (Red2 fluorescence).

Increasing miRNA-4723 levels and inhibiting miRNA-485 resulted in ~45-50% reduction of Aβ oligomer association with the cellular surface when compared to scrambled miRNA (Fig. 3.9). On the other hand, inhibiting miRNA-4723 and increasing the amounts of miRNA-485 in cells seems to be less protective against Aβ oligomer binding with up to ~20% more Aβ oligomers at the surface of SY5Y when compared to miRNA-4723 mimic and miRNA-485 inhibitor.

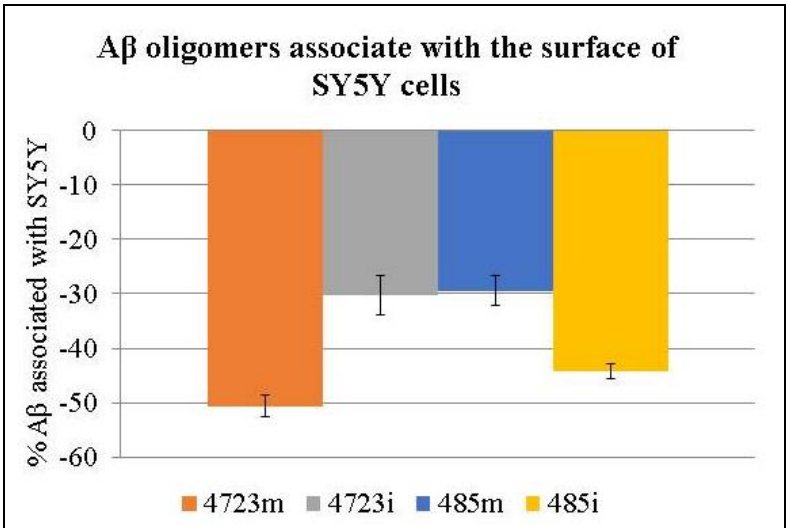

Figure 3.9. Alexa-647 labeled Aβ oligomers interact with the surface of SY5Y cells transfected with mimics or inhibitors. SY5Y were incubated with 2 μM Aβ oligomers and analyzed with flow cytometry. SY5Y cells were transfected with scrambled miRNA as a control; levels of Aβ binding to scrambled-transfected cells are set at zero. Average of three experiments with standard error is displayed. m – mimic, i – inhibitor.

To summarize the data so far, as a result of proteomic study, specific miRNAs were identified as potential drivers of the protein changes observed at the PSDs of NDAN vs. AD.

MiRNA target engagement in vivo

Wild-type B6 mice were injected with miRNA positive controls to determine target engagement *in vivo*. Control mice received injection of artificial cerebrospinal fluid (aCSF), while the two experimental groups received varying amounts of miRNA mimic (0.2-1 nmole) and inhibitor (0.2 and 0.4 nmole).

Hsa-let-7c inhibitor targets HMGA2. HMGA2 (High Mobility Group AT-Hook 2) is a transcription factor, which plays an important role during chromosome condensation during

meiotic G2/M transition. Two concentrations of the inhibitor were tested: 0.2 and 0.4 nmole/injection. Levels of HMGA2 were increased in hippocampus and frontal cortex in response to let-7c inhibitor injection (Fig. 3.10). Significant reduction of HMGA2 levels was observed when 0.4 nmole/injection was delivered ICV.

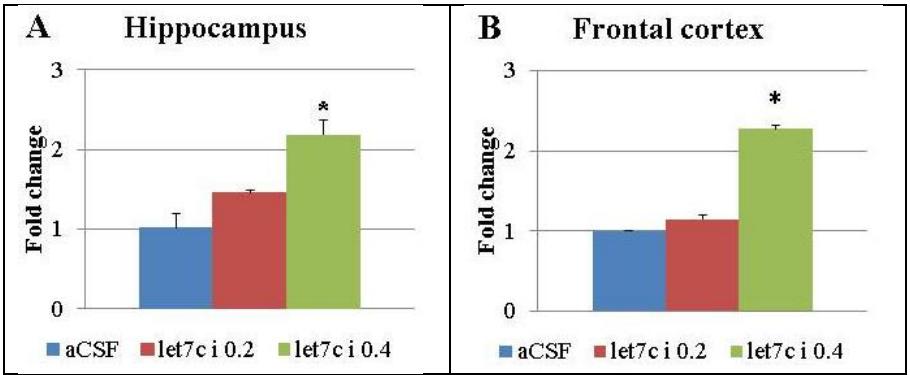

Figure 3.10. HMGA2 mRNA levels in hippocampus and frontal cortex of mice injected ICV with let-7c inhibitor. HMGA2 levels increase with the increasing concentration of let-7c inhibitor in (A) hippocampus and (B) frontal cortex. n=2, technical replicates. * - $p<0.05$ vs. aCSF, t-test. Error bars represent standard deviation.

MiRNA-1 mimic targets TWF1. TWF1 (Twinfilin-1) is an actin-binding protein involved in motile and morphological processes. Five concentrations of the mimic were tested: 0.2, 0.4, 0.6, 0.8 and 1 nmole/injection. ICV injection of at least 0.4 nmole of miRNA-1 mimic resulted in downregulation of TWF1 (Fig. 3.11). However, 0.2 nmole/injection yields and in increase in TWF1 levels. We have observed a similar phenomenon in another experiment with different miRNA mimic (not shown here). This could be due to compensatory mechanisms that rescue the RNA transcription, leading to increased production of target mRNA.

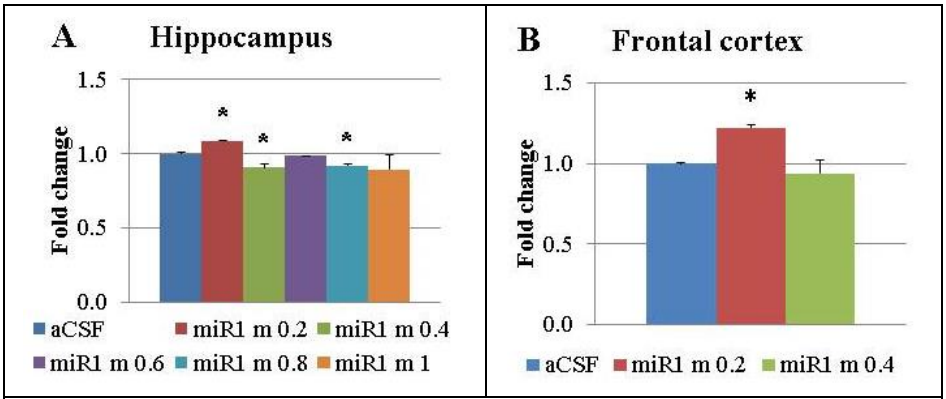

Figure 3.11. TWF1 mRNA levels in hippocampus and frontal cortex of mice injected ICV with miRNA-1 mimic. TWF1 levels decrease in (A) hippocampus and (B) frontal cortex when sufficient amount of miRNA-1 mimic is delivered ICV. n=2, technical replicates. * - $p<0.05$ vs. aCSF, t-test. Error bars represent standard deviation.

Effect of miRNA on Aβ binding to synaptosomes

In order to determine if the selected miRNAs have an effect on Aβ oligomer binding to the synaptosomes, wild-type B6 mice received an ICV injection of 1 nmole of selected miRNA mimics or inhibitors. At 24 hours post-injection, the brain regions were collected for analysis. The synaptosomes were isolated from the hippocampi and frontal cortex and Aβ oligomer binding was analyzed by flow cytometry.

When we analyzed the Aβ binding to the synaptosomes isolated from hippocampi, we determined that modulation of selected miRNAs results in 7-35% decrease in binding when compared to mice injected with scrambled miRNA (Fig. 3.12).

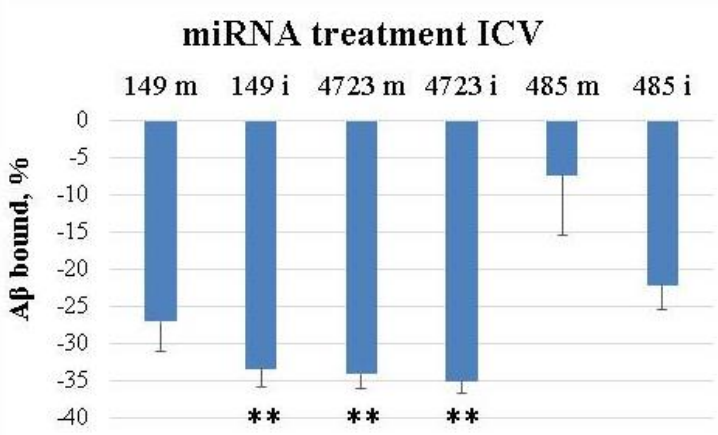

Figure 3.12. Aβ binding to synaptosomes is decreased in female mice after ICV treatment with selected miRNA mimics or inhibitors. As a control, mice received scrambled miRNA ICV; levels of Aβ binding to scrambled-injected mice are set at zero. n=7. ** - $p<0.01$ vs. scrambled miRNA, t-test. Error bars represent standard error.

Discussion

We have focused on several miRNAs (4723, 149 and 485) to test their role in modulation of Aβ oligomer binding to the synapses. These miRNAs were selected based on the analysis of the post-synaptic density proteome of NDAN vs. AD and healthy age-matched control individuals. MiRNA-4723, -485 and -149 were identified by the IPA Upstream regulators tool which was used to determine the drivers of the differential protein expression at the PSDs of NDAN, AD and control. These molecules are involved in regulation of gene expression, with each miRNA targeting multiple mRNAs. Interestingly, the miRNAs predicted by IPA are involved in the regulation of synaptic genes [194-197, 200]. We have measured these miRNAs in post-mortem human frontal cortices to confirm the IPA prediction. Indeed, the three selected miRNAs were found to be differentially expressed in control, AD and NDAN. MiRNA-149 (Fig. 3.4A) and -485 (Fig. 3.4B) are upregulated in AD, while -4723 is below detection limit in AD with no change in NDAN (Fig. 3.4C). MiRNA-485 is significantly downregulated in NDAN vs. control (Fig. 3.4B).

In order to further study these miRNAs we used SH-SY5Y cells. Interestingly, the levels of endogenous miRNA-4723, -149 and -485 were downregulated by Aβ oligomers (Fig. 3.6). Others report changes in miRNA levels as a result of Aβ action. Schonrock *et al*. showed that 47% of all miRNAs they have tested were downregulated after treatment with Aβ oligomers [201]. MiRNA downregulation by Aβ oligomers occurs rapidly [201]. The half-life of miRNAs as well as their turnover varies from 1 to > 24 hours [202, 203], which indicates that miRNAs are very carefully regulated potent molecules that can alter gene expression.

MiRNA dysregulation is studied in several disorders [204, 205], AD being one of them [40, 178-181]. MiRNAs have been proposed to be used as biomarkers in AD [179] since they can be detected in body fluids (reviewed in [177, 179, 206]). However, it remains unclear if that is a cause or a consequence of the disease state. Aβ oligomers are known modulators of synaptic plasticity [22, 207]. On the other hand, multiple miRNAs have been reported to play a role in synaptic plasticity (*i.e.* miRNA-9, -132, -134, -138, -125 and other) ([197], reviewed in [203, 208, 209]). MiRNAs are capable of regulating both functional and structural plasticity, thus impacting the neural development, physiological function, and possibly the disease pathogenesis. It is then tempting to speculate that the balance and fine regulation of miRNA levels are important factors which can determine the sensitivity of synapses to Aβ oligomers. In fact, we observed reduced binding of Aβ oligomers to the cellular surface when SH-SY5Y cells were treated with either mimic of inhibitor of miRNA-485 and -4723 (Fig. 3.9). To the best of our knowledge, these experiments for the first time address the role of miRNAs in Aβ binding to the synapses.

Most importantly, when we altered the levels of selected miRNAs (4723, 485 and 149) by injecting the mimic or inhibitor ICV, we observed a downregulation of Aβ oligomer binding to the synaptosomes (Fig. 3.12). Interestingly, miRNA-485 (mimic, in particular) does not seem to protect synapses from Aβ binding as effectively as miRNA-4723 or -149.

So far we have tested the miRNA mimics and inhibitors in females, however, the experiments with males could provide additional information regarding the effect of miRNA on Aβ binding. Additionally, since the possibility of the selected miRNAs converging onto the same (or related) pathways cannot be eliminated, it would be important to test the combinations of

selected miRNAs and their role on Aβ binding to the synapses when delivered as a combination therapy.

MiRNA are powerful tools that can modify gene expression resulting in altered protein levels. Pioneering work by Alvarez-Erviti *et al.* demonstrates that miRNAs can be delivered to brain via systemic injection of exosomes [210]. While more research is needed to advance our understanding of miRNA biogenesis, regulation and verification of potential targets, they pose as attractive therapeutic targets.

CONCLUSION AND FUTURE DIRECTIONS

Alzheimer's disease (AD) is a terminal neurodegenerative disorder which is characterized by accumulation of amyloid plaques and neurofibrillary tangles in central nervous system. Nevertheless, certain individuals remain cognitively intact despite manifestation of substantial plaques and tangles consistent with what would be normally associated with fully symptomatic AD. Here referred to as Non-Demented with Alzheimer's Neuropathology – NDAN.

The aim of this project was to determine if the PSD of NDAN subjects has a unique protein signature, consistent with their unique ability to reject the toxic Aβ oligomers, and to test if differential expression of miRNAs is driving the protein expression at the PSDs.

Subcellular fractionation combined with 2DE and mass spectrometry protein identification was used to study the postsynaptic density proteome of the hippocampus from cognitively intact NDAN subjects in comparison to demented AD patients and healthy age-matched controls. Fifteen unique proteins set NDAN apart from AD, thus supporting the notion that NDAN individuals are distinct from both control subjects and AD patients, and should likely not be considered pre-AD. The subset of proteins identified in this study can be further investigated in order to establish the mechanisms responsible for preservation of cognitive function in NDAN despite the presence of AD pathology. Additional analysis of post-translational modifications would be of interest as it can yield more insights into the protective mechanisms at play in NDAN, which in turn can result in development of novel therapeutic targets.

Next, the contribution of miRNAs to the extraordinary ability of NDAN synapses to become resilient to damaging effects of Aβ oligomers was evaluated. I studied selected miRNAs

(149, 485 and 4723) and their role on Aβ oligomer binding *in vitro* (in SH-SY5Y cells) and *in vivo* (ICV injections in wild-type mice). It was determined that in females the modulation of miRNA levels *in vivo* results in decreased Aβ oligomer binding to the synapses. In future, modulation of miRNA-4723, -485 and -149 levels should be tested in male mice to determine if these miRNAs have a similar effect on oligomer binding in males. Treatment with combinations of miRNA mimics and inhibitors could provide additional insight to help define the role of selected miRNA in the synaptic binding of Aβ oligomers. It would also be interesting to assess if modulation of these miRNAs has an effect on electrophysiological properties of Schaffer collateral pathway in the hippocampus.

Mechanisms that allow NDAN subjects to escape dementia remain unresolved and understanding such protective biological processes could reveal novel targets for the development of effective treatments for AD.

REFERENCES

1. Alzheimer'sAssociation. (2015). 2015 Alzheimer's Disease Facts and Figures. (225 N. Michigan Ave., Fl. 17, Chicago, IL 60601: Alzheimer's Association).

2. Aging NIo. (2012). Preventing Alzheimer's Disease: What Do We Know? (31 Center Drive, MSC 2292, Bethesda, MD 20892: National Institute on Aging).

3. Maarouf CL, Daugs ID, Kokjohn TA, Walker DG, Hunter JM, Kruchowsky JC, Woltjer R, Kaye J, Castaño EM, Sabbagh MN, Beach TG and Roher AE. Alzheimer's disease and non-demented high pathology control nonagenarians: comparing and contrasting the biochemistry of cognitively successful aging. PLoS One. 2011; 6(11):e27291.

4. Matrone C, Djelloul M, Taglialatela G and Perrone L. Inflammatory risk factors and pathologies promoting Alzheimer`s disease progression: is RAGE the key? Histol Histopathol. 2014.

5. Association As. (2014). Alzheimer's Facts and Figures. (225 N. Michigan Ave., Fl. 17, Chicago, IL 60601: Alzheimer's Association).

6. Yaari R and Corey-Bloom J. Alzheimer's disease. Semin Neurol. 2007; 27(1):32-41.

7. Kim GH, Jeon S, Seo SW, Kim MJ, Kim JH, Roh JH, Shin JS, Kim CH, Im K, Lee JM, Qiu A, Kim ST and Na DL. Topography of cortical thinning areas associated with hippocampal atrophy (HA) in patients with Alzheimer's disease (AD). Arch Gerontol Geriatr. 2012; 54(2):e122-129.

8. Vandenberghe R. The Relationship between Amyloid Deposition, Neurodegeneration, and Cognitive Decline in Dementia. Curr Neurol Neurosci Rep. 2014; 14(11):498.

9. Picone P, Nuzzo D, Caruana L, Scafidi V and Di Carlo M. Mitochondrial dysfunction: different routes to Alzheimer's disease therapy. Oxid Med Cell Longev. 2014; 2014:780179.

10. Karran E, Mercken M and De Strooper B. The amyloid cascade hypothesis for Alzheimer's disease: an appraisal for the development of therapeutics. Nat Rev Drug Discov. 2011; 10(9):698-712.

11. Aisenbrey C, Borowik T, Byström R, Bokvist M, Lindström F, Misiak H, Sani MA and Gröbner G. How is protein aggregation in amyloidogenic diseases modulated by biological membranes? Eur Biophys J. 2008; 37(3):247-255.

12. Aizenstein HJ, Nebes RD, Saxton JA, Price JC, Mathis CA, Tsopelas ND, Ziolko SK, James JA, Snitz BE, Houck PR, Bi W, Cohen AD, Lopresti BJ, et al. Frequent amyloid deposition without significant cognitive impairment among the elderly. Arch Neurol. 2008; 65(11):1509-1517.

13. Gómez-Isla T, Hollister R, West H, Mui S, Growdon JH, Petersen RC, Parisi JE and Hyman BT. Neuronal loss correlates with but exceeds neurofibrillary tangles in Alzheimer's disease. Ann Neurol. 1997; 41(1):17-24.

14. Stains CI, Mondal K and Ghosh I. Molecules that target beta-amyloid. ChemMedChem. 2007; 2(12):1674-1692.

15. Guerrero-Muñoz MJ, Gerson J and Castillo-Carranza DL. Tau Oligomers: The Toxic Player at Synapses in Alzheimer's Disease. Front Cell Neurosci. 2015; 9:464.

16. Lasagna-Reeves CA, Castillo-Carranza DL, Sengupta U, Sarmiento J, Troncoso J, Jackson GR and Kayed R. Identification of oligomers at early stages of tau aggregation in Alzheimer's disease. FASEB J. 2012; 26(5):1946-1959.

17. Reese LC, Zhang W, Dineley KT, Kayed R and Taglialatela G. Selective induction of calcineurin activity and signaling by oligomeric amyloid beta. Aging Cell. 2008; 7(6):824-835.

18. Lacor PN, Buniel MC, Chang L, Fernandez SJ, Gong Y, Viola KL, Lambert MP, Velasco PT, Bigio EH, Finch CE, Krafft GA and Klein WL. Synaptic targeting by Alzheimer's-related amyloid beta oligomers. J Neurosci. 2004; 24(45):10191-10200.

19. Koffie RM, Meyer-Luehmann M, Hashimoto T, Adams KW, Mielke ML, Garcia-Alloza M, Micheva KD, Smith SJ, Kim ML, Lee VM, Hyman BT and Spires-Jones TL. Oligomeric amyloid beta associates with postsynaptic densities and correlates with excitatory synapse loss near senile plaques. Proc Natl Acad Sci U S A. 2009; 106(10):4012-4017.

20. Lasagna-Reeves CA, Castillo-Carranza DL, Sengupta U, Clos AL, Jackson GR and Kayed R. Tau oligomers impair memory and induce synaptic and mitochondrial dysfunction in wild-type mice. Mol Neurodegener. 2011; 6:39.

21. Chabrier MA, Cheng D, Castello NA, Green KN and LaFerla FM. Synergistic effects of amyloid-beta and wild-type human tau on dendritic spine loss in a floxed double transgenic model of Alzheimer's disease. Neurobiol Dis. 2014; 64:107-117.

22. Dineley KT, Kayed R, Neugebauer V, Fu Y, Zhang W, Reese LC and Taglialatela G. Amyloid-beta oligomers impair fear conditioned memory in a calcineurin-dependent fashion in mice. J Neurosci Res. 2010; 88(13):2923-2932.

23. Rhein V, Song X, Wiesner A, Ittner LM, Baysang G, Meier F, Ozmen L, Bluethmann H, Dröse S, Brandt U, Savaskan E, Czech C, Götz J, et al. Amyloid-beta and tau synergistically impair the oxidative phosphorylation system in triple transgenic Alzheimer's disease mice. Proc Natl Acad Sci U S A. 2009; 106(47):20057-20062.

24. Nixon RA. Autophagy, amyloidogenesis and Alzheimer disease. J Cell Sci. 2007; 120(Pt 23):4081-4091.

25. Markesbery WR. Oxidative stress hypothesis in Alzheimer's disease. Free Radic Biol Med. 1997; 23(1):134-147.

26. Philipps V, Amieva H, Andrieu S, Dufouil C, Berr C, Dartigues JF, Jacqmin-Gadda H and Proust-Lima C. Normalized Mini-Mental State Examination for Assessing Cognitive Change in Population-Based Brain Aging Studies. Neuroepidemiology. 2014; 43(1):15-25.

27. Consensus recommendations for the postmortem diagnosis of Alzheimer's disease. The National Institute on Aging, and Reagan Institute Working Group on Diagnostic Criteria for the Neuropathological Assessment of Alzheimer's Disease. Neurobiol Aging. 1997; 18(4 Suppl):S1-2.

28. Braak H and Braak E. Neuropathological stageing of Alzheimer-related changes. Acta Neuropathol. 1991; 82(4):239-259.

29. Dahms SO, Hoefgen S, Roeser D, Schlott B, Gührs KH and Than ME. Structure and biochemical analysis of the heparin-induced E1 dimer of the amyloid precursor protein. Proc Natl Acad Sci U S A. 2010; 107(12):5381-5386.

30. Lazarov O and Demars MP. All in the Family: How the APPs Regulate Neurogenesis. Front Neurosci. 2012; 6:81.

31. Del Prete D, Lombino F, Liu X and D'Adamio L. APP Is Cleaved by Bace1 in Pre-Synaptic Vesicles and Establishes a Pre-Synaptic Interactome, via Its Intracellular Domain, with Molecular Complexes that Regulate Pre-Synaptic Vesicles Functions. PLoS One. 2014; 9(9):e108576.

32. Jonsson T, Atwal JK, Steinberg S, Snaedal J, Jonsson PV, Bjornsson S, Stefansson H, Sulem P, Gudbjartsson D, Maloney J, Hoyte K, Gustafson A, Liu Y, et al. A mutation in APP

protects against Alzheimer's disease and age-related cognitive decline. Nature. 2012; 488(7409):96-99.

33. Vetrivel KS and Thinakaran G. Amyloidogenic processing of beta-amyloid precursor protein in intracellular compartments. Neurology. 2006; 66(2 Suppl 1):S69-73.

34. Nunan J and Small DH. Regulation of APP cleavage by alpha-, beta- and gamma-secretases. FEBS Lett. 2000; 483(1):6-10.

35. Vassar R, Bennett BD, Babu-Khan S, Kahn S, Mendiaz EA, Denis P, Teplow DB, Ross S, Amarante P, Loeloff R, Luo Y, Fisher S, Fuller J, et al. Beta-secretase cleavage of Alzheimer's amyloid precursor protein by the transmembrane aspartic protease BACE. Science. 1999; 286(5440):735-741.

36. Cole SL and Vassar R. The Alzheimer's disease beta-secretase enzyme, BACE1. Mol Neurodegener. 2007; 2:22.

37. Reese LC, Laezza F, Woltjer R and Taglialatela G. Dysregulated phosphorylation of Ca(2+) /calmodulin-dependent protein kinase II-α in the hippocampus of subjects with mild cognitive impairment and Alzheimer's disease. J Neurochem. 2011; 119(4):791-804.

38. Sperling RA, Aisen PS, Beckett LA, Bennett DA, Craft S, Fagan AM, Iwatsubo T, Jack CR, Kaye J, Montine TJ, Park DC, Reiman EM, Rowe CC, et al. Toward defining the preclinical stages of Alzheimer's disease: recommendations from the National Institute on Aging-Alzheimer's Association workgroups on diagnostic guidelines for Alzheimer's disease. Alzheimers Dement. 2011; 7(3):280-292.

39. Bjorklund NL, Reese LC, Sadagoparamanujam VM, Ghirardi V, Woltjer RL and Taglialatela G. Absence of amyloid β oligomers at the postsynapse and regulated synaptic

Zn2+ in cognitively intact aged individuals with Alzheimer's disease neuropathology. Mol Neurodegener. 2012; 7:23.

40. Briley D, Ghirardi V, Woltjer R, Renck A, Zolochevska O, Taglialatela G and Micci MA. Preserved neurogenesis in non-demented individuals with AD neuropathology. Sci Rep. 2016; 6:27812.

41. Erten-Lyons D, Woltjer RL, Dodge H, Nixon R, Vorobik R, Calvert JF, Leahy M, Montine T and Kaye J. Factors associated with resistance to dementia despite high Alzheimer disease pathology. Neurology. 2009; 72(4):354-360.

42. Iacono D, O'Brien R, Resnick SM, Zonderman AB, Pletnikova O, Rudow G, An Y, West MJ, Crain B and Troncoso JC. Neuronal hypertrophy in asymptomatic Alzheimer disease. J Neuropathol Exp Neurol. 2008; 67(6):578-589.

43. Kramer PL, Xu H, Woltjer RL, Westaway SK, Clark D, Erten-Lyons D, Kaye JA, Welsh-Bohmer KA, Troncoso JC, Markesbery WR, Petersen RC, Turner RS, Kukull WA, et al. Alzheimer disease pathology in cognitively healthy elderly: a genome-wide study. Neurobiol Aging. 2011; 32(12):2113-2122.

44. Liang WS, Dunckley T, Beach TG, Grover A, Mastroeni D, Ramsey K, Caselli RJ, Kukull WA, McKeel D, Morris JC, Hulette CM, Schmechel D, Reiman EM, et al. Neuronal gene expression in non-demented individuals with intermediate Alzheimer's Disease neuropathology. Neurobiol Aging. 2010; 31(4):549-566.

45. Price JL, McKeel DW, Buckles VD, Roe CM, Xiong C, Grundman M, Hansen LA, Petersen RC, Parisi JE, Dickson DW, Smith CD, Davis DG, Schmitt FA, et al. Neuropathology of nondemented aging: presumptive evidence for preclinical Alzheimer disease. Neurobiol Aging. 2009; 30(7):1026-1036.

46. Riudavets MA, Iacono D, Resnick SM, O'Brien R, Zonderman AB, Martin LJ, Rudow G, Pletnikova O and Troncoso JC. Resistance to Alzheimer's pathology is associated with nuclear hypertrophy in neurons. Neurobiol Aging. 2007; 28(10):1484-1492.

47. Gefen T, Peterson M, Papastefan ST, Martersteck A, Whitney K, Rademaker A, Bigio EH, Weintraub S, Rogalski E, Mesulam MM and Geula C. Morphometric and histologic substrates of cingulate integrity in elders with exceptional memory capacity. J Neurosci. 2015; 35(4):1781-1791.

48. De Felice FG, Vieira MN, Bomfim TR, Decker H, Velasco PT, Lambert MP, Viola KL, Zhao WQ, Ferreira ST and Klein WL. Protection of synapses against Alzheimer's-linked toxins: insulin signaling prevents the pathogenic binding of Abeta oligomers. Proc Natl Acad Sci U S A. 2009; 106(6):1971-1976.

49. Freiherr J, Hallschmid M, Frey WH, Brünner YF, Chapman CD, Hölscher C, Craft S, De Felice FG and Benedict C. Intranasal insulin as a treatment for Alzheimer's disease: a review of basic research and clinical evidence. CNS Drugs. 2013; 27(7):505-514.

50. Dinamarca MC, Ríos JA and Inestrosa NC. Postsynaptic Receptors for Amyloid-β Oligomers as Mediators of Neuronal Damage in Alzheimer's Disease. Front Physiol. 2012; 3:464.

51. Reese LC and Taglialatela G. Neuroimmunomodulation by calcineurin in aging and Alzheimer's disease. Aging Dis. 2010; 1(3):245-253.

52. Scheff SW, Price DA, Schmitt FA, DeKosky ST and Mufson EJ. Synaptic alterations in CA1 in mild Alzheimer disease and mild cognitive impairment. Neurology. 2007; 68(18):1501-1508.

53. Zolochevska O and Taglialatela G. Non-Demented Individuals with Alzheimer's Disease Neuropathology: Resistance to Cognitive Decline May Reveal New Treatment Strategies. Curr Pharm Des. 2016; 22(26):4063-4068.

54. Lue LF, Brachova L, Civin WH and Rogers J. Inflammation, A beta deposition, and neurofibrillary tangle formation as correlates of Alzheimer's disease neurodegeneration. J Neuropathol Exp Neurol. 1996; 55(10):1083-1088.

55. Folstein MF, Folstein SE and McHugh PR. "Mini-mental state". A practical method for grading the cognitive state of patients for the clinician. J Psychiatr Res. 1975; 12(3):189-198.

56. Bjorklund NL, Sadagoparamanujam VM and Taglialatela G. Selective, quantitative measurement of releasable synaptic zinc in human autopsy hippocampal brain tissue from Alzheimer's disease patients. J Neurosci Methods. 2012; 203(1):146-151.

57. Phillips GR, Huang JK, Wang Y, Tanaka H, Shapiro L, Zhang W, Shan WS, Arndt K, Frank M, Gordon RE, Gawinowicz MA, Zhao Y and Colman DR. The presynaptic particle web: ultrastructure, composition, dissolution, and reconstitution. Neuron. 2001; 32(1):63-77.

58. Wiktorowicz JE, Stafford S, Rea H, Urvil P, Soman K, Kurosky A, Perez-Polo JR and Savidge TC. Quantification of cysteinyl S-nitrosylation by fluorescence in unbiased proteomic studies. Biochemistry. 2011; 50(25):5601-5614.

59. Wiktorowicz JE, Stafford SJ and Garg NJ. (2017). Protein Cysteinyl-S-Nitrosylation: Analysis and Quantification. In: Shukla AK, ed. Methods Enzymol. (Burlington, UK: Academic Press), pp. 1-14.

60. Pretzer E and Wiktorowicz JE. Saturation fluorescence labeling of proteins for proteomic analyses. Anal Biochem. 2008; 374(2):250-262.

61. Straub C, Pazdrak K, Young TW, Stafford SJ, Wu Z, Wiktorowicz JE, Haag AM, English RD, Soman KV and Kurosky A. Toward the Proteome of the Human Peripheral Blood Eosinophil. Proteomics Clinical Applications. 2009; 3(10):1151-1173.

62. Benjamini Y and Hochberg Y. Controlling the False Discovery Rate: a Practical and Powerful Approach to Multiple Testing. J R Stat Soc B. 1995; 57(1):289-300.

63. Allen M, Kachadoorian M, Quicksall Z, Zou F, Chai HS, Younkin C, Crook JE, Pankratz VS, Carrasquillo MM, Krishnan S, Nguyen T, Ma L, Malphrus K, et al. Association of MAPT haplotypes with Alzheimer's disease risk and MAPT brain gene expression levels. Alzheimers Res Ther. 2014; 6(4):39.

64. Singhrao SK, Thomas P, Wood JD, MacMillan JC, Neal JW, Harper PS and Jones AL. Huntingtin protein colocalizes with lesions of neurodegenerative diseases: An investigation in Huntington's, Alzheimer's, and Pick's diseases. Exp Neurol. 1998; 150(2):213-222.

65. Van Cauwenberghe C, Van Broeckhoven C and Sleegers K. The genetic landscape of Alzheimer disease: clinical implications and perspectives. Genet Med. 2016; 18(5):421-430.

66. O'Brien RJ and Wong PC. Amyloid precursor protein processing and Alzheimer's disease. Annu Rev Neurosci. 2011; 34:185-204.

67. Kelleher RJ and Shen J. Presenilin-1 mutations and Alzheimer's disease. Proc Natl Acad Sci U S A. 2017; 114(4):629-631.

68. Chen Z and Zhong C. Decoding Alzheimer's disease from perturbed cerebral glucose metabolism: implications for diagnostic and therapeutic strategies. Prog Neurobiol. 2013; 108:21-43.

69. Mi H, Lazareva-Ulitsky B, Loo R, Kejariwal A, Vandergriff J, Rabkin S, Guo N, Muruganujan A, Doremieux O, Campbell MJ, Kitano H and Thomas PD. The PANTHER

database of protein families, subfamilies, functions and pathways. Nucleic Acids Res. 2005; 33(Database issue):D284-288.

70. Thomas PD, Campbell MJ, Kejariwal A, Mi H, Karlak B, Daverman R, Diemer K, Muruganujan A and Narechania A. PANTHER: a library of protein families and subfamilies indexed by function. Genome Res. 2003; 13(9):2129-2141.

71. Huang dW, Sherman BT and Lempicki RA. Systematic and integrative analysis of large gene lists using DAVID bioinformatics resources. Nat Protoc. 2009; 4(1):44-57.

72. Gerke V and Moss SE. Annexins: from structure to function. Physiol Rev. 2002; 82(2):331-371.

73. Bamburg JR and Bernstein BW. Actin dynamics and cofilin-actin rods in alzheimer disease. Cytoskeleton (Hoboken). 2016; 73(9):477-497.

74. Rescher U and Gerke V. Annexins--unique membrane binding proteins with diverse functions. J Cell Sci. 2004; 117(Pt 13):2631-2639.

75. Gauthier-Kemper A, Weissmann C, Golovyashkina N, Sebö-Lemke Z, Drewes G, Gerke V, Heinisch JJ and Brandt R. The frontotemporal dementia mutation R406W blocks tau's interaction with the membrane in an annexin A2-dependent manner. J Cell Biol. 2011; 192(4):647-661.

76. Groenendyk J, Lynch J and Michalak M. Calreticulin, Ca2+, and calcineurin - signaling from the endoplasmic reticulum. Mol Cells. 2004; 17(3):383-389.

77. Taguchi J, Fujii A, Fujino Y, Tsujioka Y, Takahashi M, Tsuboi Y, Wada I and Yamada T. Different expression of calreticulin and immunoglobulin binding protein in Alzheimer's disease brain. Acta Neuropathol. 2000; 100(2):153-160.

78. Johnson RJ, Xiao G, Shanmugaratnam J and Fine RE. Calreticulin functions as a molecular chaperone for the beta-amyloid precursor protein. Neurobiol Aging. 2001; 22(3):387-395.

79. Vattemi G, Engel WK, McFerrin J and Askanas V. Endoplasmic reticulum stress and unfolded protein response in inclusion body myositis muscle. Am J Pathol. 2004; 164(1):1-7.

80. Michalak M, Corbett EF, Mesaeli N, Nakamura K and Opas M. Calreticulin: one protein, one gene, many functions. Biochem J. 1999; 344 Pt 2:281-292.

81. Duus K, Hansen PR and Houen G. Interaction of calreticulin with amyloid beta peptide 1-42. Protein Pept Lett. 2008; 15(1):103-107.

82. Stemmer N, Strekalova E, Djogo N, Plöger F, Loers G, Lutz D, Buck F, Michalak M, Schachner M and Kleene R. Generation of amyloid-β is reduced by the interaction of calreticulin with amyloid precursor protein, presenilin and nicastrin. PLoS One. 2013; 8(4):e61299.

83. Lynch J and Michalak M. Calreticulin is an upstream regulator of calcineurin. Biochem Biophys Res Commun. 2003; 311(4):1173-1179.

84. Lynch J, Guo L, Gelebart P, Chilibeck K, Xu J, Molkentin JD, Agellon LB and Michalak M. Calreticulin signals upstream of calcineurin and MEF2C in a critical Ca(2+)-dependent signaling cascade. J Cell Biol. 2005; 170(1):37-47.

85. Abdul HM, Sama MA, Furman JL, Mathis DM, Beckett TL, Weidner AM, Patel ES, Baig I, Murphy MP, LeVine H, Kraner SD and Norris CM. Cognitive decline in Alzheimer's disease is associated with selective changes in calcineurin/NFAT signaling. J Neurosci. 2009; 29(41):12957-12969.

86. Norris CM, Kadish I, Blalock EM, Chen KC, Thibault V, Porter NM, Landfield PW and Kraner SD. Calcineurin triggers reactive/inflammatory processes in astrocytes and is upregulated in aging and Alzheimer's models. J Neurosci. 2005; 25(18):4649-4658.

87. Ferrer I, Gómez A, Carmona M, Huesa G, Porta S, Riera-Codina M, Biagioli M, Gustincich S and Aso E. Neuronal hemoglobin is reduced in Alzheimer's disease, argyrophilic grain disease, Parkinson's disease, and dementia with Lewy bodies. J Alzheimers Dis. 2011; 23(3):537-550.

88. Wilson MT and Reeder BJ. Oxygen-binding haem proteins. Exp Physiol. 2008; 93(1):128-132.

89. Chuang JY, Lee CW, Shih YH, Yang T, Yu L and Kuo YM. Interactions between amyloid-β and hemoglobin: implications for amyloid plaque formation in Alzheimer's disease. PLoS One. 2012; 7(3):e33120.

90. van de Haar HJ, Burgmans S, Jansen JF, van Osch MJ, van Buchem MA, Muller M, Hofman PA, Verhey FR and Backes WH. Blood-Brain Barrier Leakage in Patients with Early Alzheimer Disease. Radiology. 2017; 282(2):615.

91. Ryu JK and McLarnon JG. A leaky blood-brain barrier, fibrinogen infiltration and microglial reactivity in inflamed Alzheimer's disease brain. J Cell Mol Med. 2009; 13(9A):2911-2925.

92. Ueno M, Chiba Y, Murakami R, Matsumoto K, Kawauchi M and Fujihara R. Blood-brain barrier and blood-cerebrospinal fluid barrier in normal and pathological conditions. Brain Tumor Pathol. 2016; 33(2):89-96.

93. Schelshorn DW, Schneider A, Kuschinsky W, Weber D, Krüger C, Dittgen T, Bürgers HF, Sabouri F, Gassler N, Bach A and Maurer MH. Expression of hemoglobin in rodent neurons. J Cereb Blood Flow Metab. 2009; 29(3):585-595.

94. Richter F, Meurers BH, Zhu C, Medvedeva VP and Chesselet MF. Neurons express hemoglobin alpha- and beta-chains in rat and human brains. J Comp Neurol. 2009; 515(5):538-547.

95. Shephard F, Greville-Heygate O, Marsh O, Anderson S and Chakrabarti L. A mitochondrial location for haemoglobins--dynamic distribution in ageing and Parkinson's disease. Mitochondrion. 2014; 14(1):64-72.

96. Hotulainen P and Hoogenraad CC. Actin in dendritic spines: connecting dynamics to function. J Cell Biol. 2010; 189(4):619-629.

97. Schwamborn JC and Püschel AW. The sequential activity of the GTPases Rap1B and Cdc42 determines neuronal polarity. Nat Neurosci. 2004; 7(9):923-929.

98. Melendez J, Grogg M and Zheng Y. Signaling role of Cdc42 in regulating mammalian physiology. J Biol Chem. 2011; 286(4):2375-2381.

99. Boulter E, Garcia-Mata R, Guilluy C, Dubash A, Rossi G, Brennwald PJ and Burridge K. Regulation of Rho GTPase crosstalk, degradation and activity by RhoGDI1. Nat Cell Biol. 2010; 12(5):477-483.

100. Nobes CD and Hall A. Rho, rac, and cdc42 GTPases regulate the assembly of multimolecular focal complexes associated with actin stress fibers, lamellipodia, and filopodia. Cell. 1995; 81(1):53-62.

101. Tapon N and Hall A. Rho, Rac and Cdc42 GTPases regulate the organization of the actin cytoskeleton. Curr Opin Cell Biol. 1997; 9(1):86-92.

102. Vlkolinský R, Cairns N, Fountoulakis M and Lubec G. Decreased brain levels of 2',3'-cyclic nucleotide-3'-phosphodiesterase in Down syndrome and Alzheimer's disease. Neurobiol Aging. 2001; 22(4):547-553.

103. Thompson RJ. 2',3'-cyclic nucleotide-3'-phosphohydrolase and signal transduction in central nervous system myelin. Biochem Soc Trans. 1992; 20(3):621-626.

104. Lee J, Gravel M, Zhang R, Thibault P and Braun PE. Process outgrowth in oligodendrocytes is mediated by CNP, a novel microtubule assembly myelin protein. J Cell Biol. 2005; 170(4):661-673.

105. Donovan LE, Higginbotham L, Dammer EB, Gearing M, Rees HD, Xia Q, Duong DM, Seyfried NT, Lah JJ and Levey AI. Analysis of a membrane-enriched proteome from postmortem human brain tissue in Alzheimer's disease. Proteomics Clin Appl. 2012; 6(3-4):201-211.

106. Osaka H, Wang YL, Takada K, Takizawa S, Setsuie R, Li H, Sato Y, Nishikawa K, Sun YJ, Sakurai M, Harada T, Hara Y, Kimura I, et al. Ubiquitin carboxy-terminal hydrolase L1 binds to and stabilizes monoubiquitin in neuron. Hum Mol Genet. 2003; 12(16):1945-1958.

107. Liu Y, Fallon L, Lashuel HA, Liu Z and Lansbury PT. The UCH-L1 gene encodes two opposing enzymatic activities that affect alpha-synuclein degradation and Parkinson's disease susceptibility. Cell. 2002; 111(2):209-218.

108. Satoh JI and Kuroda Y. Ubiquitin C-terminal hydrolase-L1 (PGP9.5) expression in human neural cell lines following induction of neuronal differentiation and exposure to cytokines, neurotrophic factors or heat stress. Neuropathol Appl Neurobiol. 2001; 27(2):95-104.

109. Choi J, Levey AI, Weintraub ST, Rees HD, Gearing M, Chin LS and Li L. Oxidative modifications and down-regulation of ubiquitin carboxyl-terminal hydrolase L1 associated with idiopathic Parkinson's and Alzheimer's diseases. J Biol Chem. 2004; 279(13):13256-13264.

110. Lombardino AJ, Li XC, Hertel M and Nottebohm F. Replaceable neurons and neurodegenerative disease share depressed UCHL1 levels. Proc Natl Acad Sci U S A. 2005; 102(22):8036-8041.

111. Ghosh A and Giese KP. Calcium/calmodulin-dependent kinase II and Alzheimer's disease. Mol Brain. 2015; 8(1):78.

112. Gu Z, Liu W and Yan Z. {beta}-Amyloid impairs AMPA receptor trafficking and function by reducing Ca2+/calmodulin-dependent protein kinase II synaptic distribution. J Biol Chem. 2009; 284(16):10639-10649.

113. Wang YJ, Chen GH, Hu XY, Lu YP, Zhou JN and Liu RY. The expression of calcium/calmodulin-dependent protein kinase II-alpha in the hippocampus of patients with Alzheimer's disease and its links with AD-related pathology. Brain Res. 2005; 1031(1):101-108.

114. Lisman J, Schulman H and Cline H. The molecular basis of CaMKII function in synaptic and behavioural memory. Nat Rev Neurosci. 2002; 3(3):175-190.

115. Kennedy MB. Signal-processing machines at the postsynaptic density. Science. 2000; 290(5492):750-754.

116. Kuiper JW, Oerlemans FT, Fransen JA and Wieringa B. Creatine kinase B deficient neurons exhibit an increased fraction of motile mitochondria. BMC Neurosci. 2008; 9:73.

117. Schlattner U, Tokarska-Schlattner M and Wallimann T. Mitochondrial creatine kinase in human health and disease. Biochim Biophys Acta. 2006; 1762(2):164-180.

118. Brady ST and Lasek RJ. Nerve-specific enolase and creatine phosphokinase in axonal transport: soluble proteins and the axoplasmic matrix. Cell. 1981; 23(2):515-523.

119. Swerdlow RH, Burns JM and Khan SM. The Alzheimer's disease mitochondrial cascade hypothesis. J Alzheimers Dis. 2010; 20 Suppl 2:S265-279.

120. Moreira PI, Carvalho C, Zhu X, Smith MA and Perry G. Mitochondrial dysfunction is a trigger of Alzheimer's disease pathophysiology. Biochim Biophys Acta. 2010; 1802(1):2-10.

121. Gray LR, Tompkins SC and Taylor EB. Regulation of pyruvate metabolism and human disease. Cell Mol Life Sci. 2014; 71(14):2577-2604.

122. Tiwari V and Patel AB. Pyruvate carboxylase and pentose phosphate fluxes are reduced in AβPP-PS1 mouse model of Alzheimer's disease: a ^{13}C NMR study. J Alzheimers Dis. 2014; 41(2):387-399.

123. Nakamura Y, Takeda M, Yoshimi K, Hattori H, Hariguchi S, Kitajima S, Hashimoto S and Nishimura T. Involvement of clathrin light chains in the pathology of Alzheimer's disease. Acta Neuropathol. 1994; 87(1):23-31.

124. Tojima T, Itofusa R and Kamiguchi H. Asymmetric clathrin-mediated endocytosis drives repulsive growth cone guidance. Neuron. 2010; 66(3):370-377.

125. Kuboyama T, Lee YA, Nishiko H and Tohda C. Inhibition of clathrin-mediated endocytosis prevents amyloid β-induced axonal damage. Neurobiol Aging. 2015; 36(5):1808-1819.

126. Qin S, Hu XY, Xu H and Zhou JN. Regional alteration of synapsin I in the hippocampal formation of Alzheimer's disease patients. Acta Neuropathol. 2004; 107(3):209-215.

127. Nestler EJ and Greengard P. Distribution of protein I and regulation of its state of phosphorylation in the rabbit superior cervical ganglion. J Neurosci. 1982; 2(8):1011-1023.

128. Pevsner J, Hsu SC and Scheller RH. n-Sec1: a neural-specific syntaxin-binding protein. Proc Natl Acad Sci U S A. 1994; 91(4):1445-1449.

129. Misura KM, Scheller RH and Weis WI. Three-dimensional structure of the neuronal-Sec1-syntaxin 1a complex. Nature. 2000; 404(6776):355-362.

130. Butterfield DA, Hardas SS and Lange ML. Oxidatively modified glyceraldehyde-3-phosphate dehydrogenase (GAPDH) and Alzheimer's disease: many pathways to neurodegeneration. J Alzheimers Dis. 2010; 20(2):369-393.

131. Schulze H, Schuler A, Stüber D, Döbeli H, Langen H and Huber G. Rat brain glyceraldehyde-3-phosphate dehydrogenase interacts with the recombinant cytoplasmic domain of Alzheimer's beta-amyloid precursor protein. J Neurochem. 1993; 60(5):1915-1922.

132. Mazzola JL and Sirover MA. Reduction of glyceraldehyde-3-phosphate dehydrogenase activity in Alzheimer's disease and in Huntington's disease fibroblasts. J Neurochem. 2001; 76(2):442-449.

133. Shi Q, Xu H, Kleinman WA and Gibson GE. Novel functions of the alpha-ketoglutarate dehydrogenase complex may mediate diverse oxidant-induced changes in mitochondrial enzymes associated with Alzheimer's disease. Biochim Biophys Acta. 2008; 1782(4):229-238.

134. Shi Q and Gibson GE. Up-regulation of the mitochondrial malate dehydrogenase by oxidative stress is mediated by miR-743a. J Neurochem. 2011; 118(3):440-448.

135. Ntsapi C and Loos B. Caloric restriction and the precision-control of autophagy: A strategy for delaying neurodegenerative disease progression. Exp Gerontol. 2016; 83:97-111.

136. Balasubramanian P, Howell PR and Anderson RM. Aging and Caloric Restriction Research: A Biological Perspective With Translational Potential. EBioMedicine. 2017; 21:37-44.

137. Knoops B, Clippe A, Bogard C, Arsalane K, Wattiez R, Hermans C, Duconseille E, Falmagne P and Bernard A. Cloning and characterization of AOEB166, a novel mammalian antioxidant enzyme of the peroxiredoxin family. J Biol Chem. 1999; 274(43):30451-30458.

138. Silva AR, Santos AC, Farfel JM, Grinberg LT, Ferretti RE, Campos AH, Cunha IW, Begnami MD, Rocha RM, Carraro DM, de Bragança Pereira CA, Jacob-Filho W and Brentani H. Repair of oxidative DNA damage, cell-cycle regulation and neuronal death may influence the clinical manifestation of Alzheimer's disease. PLoS One. 2014; 9(6):e99897.

139. Dubuisson M, Vander Stricht D, Clippe A, Etienne F, Nauser T, Kissner R, Koppenol WH, Rees JF and Knoops B. Human peroxiredoxin 5 is a peroxynitrite reductase. FEBS Lett. 2004; 571(1-3):161-165.

140. Davey GP and Bolaños JP. Peroxiredoxin 5 links mitochondrial redox signalling with calcium dynamics: impact on Parkinson's disease. J Neurochem. 2013; 125(3):332-333.

141. Trujillo M, Clippe A, Manta B, Ferrer-Sueta G, Smeets A, Declercq JP, Knoops B and Radi R. Pre-steady state kinetic characterization of human peroxiredoxin 5: taking

advantage of Trp84 fluorescence increase upon oxidation. Arch Biochem Biophys. 2007; 467(1):95-106.

142. Kelly BL, Vassar R and Ferreira A. Beta-amyloid-induced dynamin 1 depletion in hippocampal neurons. A potential mechanism for early cognitive decline in Alzheimer disease. J Biol Chem. 2005; 280(36):31746-31753.

143. Guo CH, Senzel A, Li K and Feng ZP. De novo protein synthesis of syntaxin-1 and dynamin-1 in long-term memory formation requires CREB1 gene transcription in Lymnaea stagnalis. Behav Genet. 2010; 40(5):680-693.

144. Fà M, Staniszewski A, Saeed F, Francis YI and Arancio O. Dynamin 1 is required for memory formation. PLoS One. 2014; 9(3):e91954.

145. Zhu L, Su M, Lucast L, Liu L, Netzer WJ, Gandy SE and Cai D. Dynamin 1 regulates amyloid generation through modulation of BACE-1. PLoS One. 2012; 7(9):e45033.

146. Hol EM, Roelofs RF, Moraal E, Sonnemans MA, Sluijs JA, Proper EA, de Graan PN, Fischer DF and van Leeuwen FW. Neuronal expression of GFAP in patients with Alzheimer pathology and identification of novel GFAP splice forms. Mol Psychiatry. 2003; 8(9):786-796.

147. Shiozaki A, Tsuji T, Kohno R, Kawamata J, Uemura K, Teraoka H and Shimohama S. Proteome analysis of brain proteins in Alzheimer's disease: subproteomics following sequentially extracted protein preparation. J Alzheimers Dis. 2004; 6(3):257-268.

148. Kalló G, Emri M, Varga Z, Ujhelyi B, Tőzsér J, Csutak A and Csősz É. Changes in the Chemical Barrier Composition of Tears in Alzheimer's Disease Reveal Potential Tear Diagnostic Biomarkers. PLoS One. 2016; 11(6):e0158000.

149. Richens JL, Spencer HL, Butler M, Cantlay F, Vere KA, Bajaj N, Morgan K and O'Shea P. Rationalising the role of Keratin 9 as a biomarker for Alzheimer's disease. Sci Rep. 2016; 6:22962.

150. Richens JL, Vere KA, Light RA, Soria D, Garibaldi J, Smith AD, Warden D, Wilcock G, Bajaj N, Morgan K and O'Shea P. Practical detection of a definitive biomarker panel for Alzheimer's disease; comparisons between matched plasma and cerebrospinal fluid. Int J Mol Epidemiol Genet. 2014; 5(2):53-70.

151. Vafadar-Isfahani B, Ball G, Coveney C, Lemetre C, Boocock D, Minthon L, Hansson O, Miles AK, Janciauskiene SM, Warden D, Smith AD, Wilcock G, Kalsheker N, et al. Identification of SPARC-like 1 protein as part of a biomarker panel for Alzheimer's disease in cerebrospinal fluid. J Alzheimers Dis. 2012; 28(3):625-636.

152. Neuner SM, Wilmott LA, Hoffmann BR, Mozhui K and Kaczorowski CC. Hippocampal proteomics defines pathways associated with memory decline and resilience in normal aging and Alzheimer's disease mouse models. Behav Brain Res. 2017; 322(Pt B):288-298.

153. Jiang S, Wu J, Yang Y, Liu J, Ding Y and Ding M. Proteomic analysis of the cerebrospinal fluid in multiple sclerosis and neuromyelitis optica patients. Mol Med Rep. 2012; 6(5):1081-1086.

154. Garcia ML, Lobsiger CS, Shah SB, Deerinck TJ, Crum J, Young D, Ward CM, Crawford TO, Gotow T, Uchiyama Y, Ellisman MH, Calcutt NA and Cleveland DW. NF-M is an essential target for the myelin-directed "outside-in" signaling cascade that mediates radial axonal growth. J Cell Biol. 2003; 163(5):1011-1020.

155. Elder GA, Friedrich VL, Bosco P, Kang C, Gourov A, Tu PH, Lee VM and Lazzarini RA. Absence of the mid-sized neurofilament subunit decreases axonal calibers, levels of light neurofilament (NF-L), and neurofilament content. J Cell Biol. 1998; 141(3):727-739.

156. Yuan A, Rao MV, Veeranna and Nixon RA. Neurofilaments at a glance. J Cell Sci. 2012; 125(Pt 14):3257-3263.

157. Pollard TD, Blanchoin L and Mullins RD. Molecular mechanisms controlling actin filament dynamics in nonmuscle cells. Annu Rev Biophys Biomol Struct. 2000; 29:545-576.

158. Kinoshita A, Kinoshita M, Akiyama H, Tomimoto H, Akiguchi I, Kumar S, Noda M and Kimura J. Identification of septins in neurofibrillary tangles in Alzheimer's disease. Am J Pathol. 1998; 153(5):1551-1560.

159. Kinoshita A, Noda M and Kinoshita M. Differential localization of septins in the mouse brain. J Comp Neurol. 2000; 428(2):223-239.

160. Mostowy S and Cossart P. Septins: the fourth component of the cytoskeleton. Nat Rev Mol Cell Biol. 2012; 13(3):183-194.

161. Yan XX and Jeromin A. Spectrin Breakdown Products (SBDPs) as Potential Biomarkers for Neurodegenerative Diseases. Curr Transl Geriatr Exp Gerontol Rep. 2012; 1(2):85-93.

162. Fernández-Shaw C, Marina A, Cazorla P, Valdivieso F and Vázquez J. Anti-brain spectrin immunoreactivity in Alzheimer's disease: degradation of spectrin in an animal model of cholinergic degeneration. J Neuroimmunol. 1997; 77(1):91-98.

163. Masliah E, Iimoto DS, Saitoh T, Hansen LA and Terry RD. Increased immunoreactivity of brain spectrin in Alzheimer disease: a marker for synapse loss? Brain Res. 1990; 531(1-2):36-44.

164. Wechsler A and Teichberg VI. Brain spectrin binding to the NMDA receptor is regulated by phosphorylation, calcium and calmodulin. EMBO J. 1998; 17(14):3931-3939.

165. Steiner JP, Walke HT and Bennett V. Calcium/calmodulin inhibits direct binding of spectrin to synaptosomal membranes. J Biol Chem. 1989; 264(5):2783-2791.

166. Janke C and Bulinski JC. Post-translational regulation of the microtubule cytoskeleton: mechanisms and functions. Nat Rev Mol Cell Biol. 2011; 12(12):773-786.

167. Thievessen I, Thompson PM, Berlemont S, Plevock KM, Plotnikov SV, Zemljic-Harpf A, Ross RS, Davidson MW, Danuser G, Campbell SL and Waterman CM. Vinculin-actin interaction couples actin retrograde flow to focal adhesions, but is dispensable for focal adhesion growth. J Cell Biol. 2013; 202(1):163-177.

168. Quinlan MP. Vinculin, VASP, and profilin are coordinately regulated during actin remodeling in epithelial cells, which requires de novo protein synthesis and protein kinase signal transduction pathways. J Cell Physiol. 2004; 200(2):277-290.

169. Reinikainen KJ, Pitkänen A and Riekkinen PJ. 2',3'-cyclic nucleotide-3'-phosphodiesterase activity as an index of myelin in the post-mortem brains of patients with Alzheimer's disease. Neurosci Lett. 1989; 106(1-2):229-232.

170. Taglialatela G, Rastellini C and Cicalese L. Reduced Incidence of Dementia in Solid Organ Transplant Patients Treated with Calcineurin Inhibitors. J Alzheimers Dis. 2015; 47(2):329-333.

171. Taglialatela G, Hogan D, Zhang WR and Dineley KT. Intermediate- and long-term recognition memory deficits in Tg2576 mice are reversed with acute calcineurin inhibition. Behav Brain Res. 2009; 200(1):95-99.

172. Dineley KT, Hogan D, Zhang WR and Taglialatela G. Acute inhibition of calcineurin restores associative learning and memory in Tg2576 APP transgenic mice. Neurobiol Learn Mem. 2007; 88(2):217-224.

173. Reese LC and Taglialatela G. A role for calcineurin in Alzheimer's disease. Curr Neuropharmacol. 2011; 9(4):685-692.

174. Ohtsuka T, Shimizu K, Yamamori B, Kuroda S and Takai Y. Activation of brain B-Raf protein kinase by Rap1B small GTP-binding protein. J Biol Chem. 1996; 271(3):1258-1261.

175. Scheff SW, Price DA, Ansari MA, Roberts KN, Schmitt FA, Ikonomovic MD and Mufson EJ. Synaptic change in the posterior cingulate gyrus in the progression of Alzheimer's disease. J Alzheimers Dis. 2015; 43(3):1073-1090.

176. Korolainen MA, Auriola S, Nyman TA, Alafuzoff I and Pirttilä T. Proteomic analysis of glial fibrillary acidic protein in Alzheimer's disease and aging brain. Neurobiol Dis. 2005; 20(3):858-870.

177. Femminella GD, Ferrara N and Rengo G. The emerging role of microRNAs in Alzheimer's disease. Front Physiol. 2015; 6:40.

178. Schipper HM, Maes OC, Chertkow HM and Wang E. MicroRNA expression in Alzheimer blood mononuclear cells. Gene Regul Syst Bio. 2007; 1:263-274.

179. Cogswell JP, Ward J, Taylor IA, Waters M, Shi Y, Cannon B, Kelnar K, Kemppainen J, Brown D, Chen C, Prinjha RK, Richardson JC, Saunders AM, et al.

Identification of miRNA changes in Alzheimer's disease brain and CSF yields putative biomarkers and insights into disease pathways. J Alzheimers Dis. 2008; 14(1):27-41.

180. Lukiw WJ. Micro-RNA speciation in fetal, adult and Alzheimer's disease hippocampus. Neuroreport. 2007; 18(3):297-300.

181. Szafranski K, Abraham KJ and Mekhail K. Non-coding RNA in neural function, disease, and aging. Front Genet. 2015; 6:87.

182. Li W, Chen L, Qu X, He W, He Y, Feng C, Jia X, Zhou Y, Lv J, Liang B, Chen B and Jiang J. Unraveling the characteristics of microRNA regulation in the developmental and aging process of the human brain. BMC Med Genomics. 2013; 6:55.

183. Eacker SM, Dawson TM and Dawson VL. Understanding microRNAs in neurodegeneration. Nat Rev Neurosci. 2009; 10(12):837-841.

184. van Rooij E and Olson EN. MicroRNA therapeutics for cardiovascular disease: opportunities and obstacles. Nat Rev Drug Discov. 2012; 11(11):860-872.

185. Lugli G, Torvik VI, Larson J and Smalheiser NR. Expression of microRNAs and their precursors in synaptic fractions of adult mouse forebrain. J Neurochem. 2008; 106(2):650-661.

186. Kozomara A and Griffiths-Jones S. miRBase: integrating microRNA annotation and deep-sequencing data. Nucleic Acids Res. 2011; 39(Database issue):D152-157.

187. Kozomara A and Griffiths-Jones S. miRBase: annotating high confidence microRNAs using deep sequencing data. Nucleic Acids Res. 2014; 42(Database issue):D68-73.

188. Griffiths-Jones S, Grocock RJ, van Dongen S, Bateman A and Enright AJ. miRBase: microRNA sequences, targets and gene nomenclature. Nucleic Acids Res. 2006; 34(Database issue):D140-144.

189. Griffiths-Jones S, Saini HK, van Dongen S and Enright AJ. miRBase: tools for microRNA genomics. Nucleic Acids Res. 2008; 36(Database issue):D154-158.

190. Griffiths-Jones S. The microRNA Registry. Nucleic Acids Res. 2004; 32(Database issue):D109-111.

191. Clark WG, Vivonia CA and Baxter CF. Accurate freehand injection into the lateral brain ventricle of the conscious mouse. J Appl Physiol. 1968; 25(3):319-321.

192. Hamfjord J, Stangeland AM, Hughes T, Skrede ML, Tveit KM, Ikdahl T and Kure EH. Differential expression of miRNAs in colorectal cancer: comparison of paired tumor tissue and adjacent normal mucosa using high-throughput sequencing. PLoS One. 2012; 7(4):e34150.

193. Wang F, Ma YL, Zhang P, Shen TY, Shi CZ, Yang YZ, Moyer MP, Zhang HZ, Chen HQ, Liang Y and Qin HL. SP1 mediates the link between methylation of the tumour suppressor miR-149 and outcome in colorectal cancer. J Pathol. 2013; 229(1):12-24.

194. Pevida M, Lastra A, Hidalgo A, Baamonde A and Menéndez L. Spinal CCL2 and microglial activation are involved in paclitaxel-evoked cold hyperalgesia. Brain Res Bull. 2013; 95:21-27.

195. Cohen JE, Lee PR and Fields RD. Systematic identification of 3'-UTR regulatory elements in activity-dependent mRNA stability in hippocampal neurons. Philos Trans R Soc Lond B Biol Sci. 2014; 369(1652).

196. Faghihi MA, Zhang M, Huang J, Modarresi F, Van der Brug MP, Nalls MA, Cookson MR, St-Laurent G and Wahlestedt C. Evidence for natural antisense transcript-mediated inhibition of microRNA function. Genome Biol. 2010; 11(5):R56.

197. Cohen JE, Lee PR, Chen S, Li W and Fields RD. MicroRNA regulation of homeostatic synaptic plasticity. Proc Natl Acad Sci U S A. 2011; 108(28):11650-11655.

198. Arora S, Saini S, Fukuhara S, Majid S, Shahryari V, Yamamura S, Chiyomaru T, Deng G, Tanaka Y and Dahiya R. MicroRNA-4723 inhibits prostate cancer growth through inactivation of the Abelson family of nonreceptor protein tyrosine kinases. PLoS One. 2013; 8(11):e78023.

199. Alvarez AR, Sandoval PC, Leal NR, Castro PU and Kosik KS. Activation of the neuronal c-Abl tyrosine kinase by amyloid-beta-peptide and reactive oxygen species. Neurobiol Dis. 2004; 17(2):326-336.

200. Gonzalez-Zuñiga M, Contreras PS, Estrada LD, Chamorro D, Villagra A, Zanlungo S, Seto E and Alvarez AR. c-Abl stabilizes HDAC2 levels by tyrosine phosphorylation repressing neuronal gene expression in Alzheimer's disease. Mol Cell. 2014; 56(1):163-173.

201. Schonrock N, Ke YD, Humphreys D, Staufenbiel M, Ittner LM, Preiss T and Götz J. Neuronal microRNA deregulation in response to Alzheimer's disease amyloid-beta. PLoS One. 2010; 5(6):e11070.

202. Marzi MJ, Ghini F, Cerruti B, de Pretis S, Bonetti P, Giacomelli C, Gorski MM, Kress T, Pelizzola M, Muller H, Amati B and Nicassio F. Degradation dynamics of microRNAs revealed by a novel pulse-chase approach. Genome Res. 2016; 26(4):554-565.

203. Aksoy-Aksel A, Zampa F and Schratt G. MicroRNAs and synaptic plasticity--a mutual relationship. Philos Trans R Soc Lond B Biol Sci. 2014; 369(1652).

204. Im HI and Kenny PJ. MicroRNAs in neuronal function and dysfunction. Trends Neurosci. 2012; 35(5):325-334.

205. Danborg PB, Simonsen AH, Waldemar G and Heegaard NH. The potential of microRNAs as biofluid markers of neurodegenerative diseases--a systematic review. Biomarkers. 2014; 19(4):259-268.

206. van Rooij E. The art of microRNA research. Circ Res. 2011; 108(2):219-234.

207. Parihar MS and Brewer GJ. Amyloid-β as a modulator of synaptic plasticity. J Alzheimers Dis. 2010; 22(3):741-763.

208. Ye Y, Xu H, Su X and He X. Role of MicroRNA in Governing Synaptic Plasticity. Neural Plast. 2016; 2016:4959523.

209. Eacker SM, Dawson TM and Dawson VL. The interplay of microRNA and neuronal activity in health and disease. Front Cell Neurosci. 2013; 7:136.

210. Alvarez-Erviti L, Seow Y, Yin H, Betts C, Lakhal S and Wood MJ. Delivery of siRNA to the mouse brain by systemic injection of targeted exosomes. Nat Biotechnol. 2011; 29(4):341-345.

LIST OF ABBREVIATIONS

2DGE – 2D gel electrophoresis

AChE – acetylcholine receptor

aCSF – artificial cerebral spinal fluid

AD – Alzheimer's Disease

AICD – amyloid precursor protein intracellular domain

APOE – apolipoprotein ε

APP – amyloid precursor protein

Aβ – amyloid beta

BACE1 – beta-secretase 1

BRI2/ITM2B – integral membrane protein 2B

c-Abl – Abelson family of nonreceptor tyrosine kinases

CaMKII – Ca^{2+}/calmodulin-dependent protein kinase II

Ccbe1 – collagen and calcium binding EGF domains 1

cDNA – complementary DNA

CNS – central nervous system

CREB – cAMP response element-binding protein factor

CSF – cerebrospinal fluid

DAVID – Database for Annotation, Visualization and Integrated Discovery

Dlg4 – disks large homolog 4

DMEM – Dulbecco's modified Eagle's medium

Dnajb12 – DnaJ homolog subfamily B member 12

Dnm1 – dynamin 1

FDA – Food and Drug Administration

HAT – histone acetyltransferases

HDAC – histone deacetylase

ICV - intracerebroventricular

IPA – Ingenuity Pathway Analysis

Lrp11 – low density lipoprotein receptor-related protein 11

LTP – long-term potentiation

MALDI – matrix-assisted laser desorption/ionization

MAP2 – microtubule-associated protein 2

Mapt – microtubule-associated protein tau

MCI – mild cognitive impairment

miRNA – micro RNA

MMSE – mini-metal state exam

mRNA – messenger RNA

NDAN – Non-Demented with Alzheimer's Neuropathology

NFTs – neurofibrillary tangles

NIH-OHSU – National Institute of Health Oregon Health&Science University

NL-1 – neuroligin-1

NMDAR - N-methyl-D-aspartate receptor

Pacs1 – phosphofurin acidic cluster sorting protein 1

PANTHER – Protein Analysis THrough Evolutionary Relationships

Ppp3ca – protein phosphatase 3, catalytic subunit, alpha isoform

pre-miRNA – premature microRNA

pri-miRNA – primary microRNA

PrPc – prion protein

PSD – post-synaptic density

PSEN – presenilin

qRT-PCR – quantitative real-time PCR

RISC – RNA-induced silencing complex

sAPP – soluble amyloid precursor protein

scr – scrambled

Snap25 – synaptosomal-associated protein, 25 kDa

Snca – synuclein, alpha

SNO – S-Nitrosylation

Sp1 – specificity protein 1

SV2A – synaptic vesicle glycoprotein 2A

Syn1 – synapsin 1

TET – ten-eleven translocation

Tet1 – tet methylcytosine dioxygenase 1

TNF-R – tumor necrosis factor receptor

TOF – time of flight

Vamp – vesicle-associated membraine protein

α7-nAChR – alpha-7 nicotinic acetylcholine receptor

SUPPLEMENTARY INFORMATION

Protein name	Accession No.	pI	MW (kD)	AD vs. control	p - Value	NDAN vs. AD	p - Value	NDAN vs. control	p - Value
Actin, cytoplasmic 2	P63261	6.31	15	-1.50	0.170	-1.49	0.351	-2.23	0.029
Annexin (Fragment)	H0YN42	8.03	30	1.55	0.404	1.83	0.358	2.85	0.099
Calcium/calmodulin-dependent protein kinase type II subunit alpha	Q9UQM7	5.84	17	1.43	0.452	1.98	0.143	2.83	0.041
Calreticulin	P27797	4.65	71	-1.15	0.335	-2.85	0.001	-3.27	0.000
Creatine kinase B-type	P12277	6.93	17	1.05	0.596	-1.98	0.001	-1.88	0.003
Creatine kinase B-type (Fragment)	G3V4N7	5	20	1.09	0.415	-2.80	0.003	-2.57	0.004
Glial fibrillary acidic protein	E9PAX3	5	20	-1.12	0.366	-4.32	0.006	-4.84	0.004
Glial fibrillary acidic protein	P14136	5.06	34	-1.44	0.030	-2.07	0.079	-2.97	0.027
Glial fibrillary acidic protein	E9PAX3	4.98	18	1.27	0.234	-1.98	0.022	-1.56	0.192
Glial fibrillary acidic protein	P14136	5.28	46	-1.32	0.440	2.15	0.010	1.63	0.108
Glial fibrillary acidic protein	P14136	5.07	37	-1.48	0.001	1.53	0.001	1.03	0.587
Glial fibrillary acidic protein	P14136	5.18	46	-1.02	0.925	2.06	0.006	2.02	0.007
Glial fibrillary acidic protein	P14136	5.43	46	-1.25	0.175	2.12	0.004	1.69	0.024
Glial fibrillary acidic protein	P14136	5.34	46	-1.23	0.145	2.18	0.001	1.77	0.003
Glial fibrillary acidic protein	P14136	5.39	46	-1.44	0.013	2.58	0.001	1.79	0.000
Glial fibrillary acidic protein (Fragment)	K7EJU1	5.61	21	-4.13	0.009	2.00	0.196	-2.07	0.073
Glyceraldehyde-3-phosphate dehydrogenase	E7EUT4	9.17	32	-6.19	0.141	6.55	0.149	1.06	0.990
Hemoglobin subunit beta	P68871	7.34	14	1.75	0.092	1.67	0.212	2.92	0.034
Hemoglobin subunit beta	P68871	7	14	1.68	0.071	1.84	0.182	3.09	0.043
Hemoglobin subunit beta	P68871	7.35	13	1.26	0.506	2.90	0.016	3.66	0.001
Isoform 1 of Vinculin	P18206-2	5.88	118	1.03	0.864	1.92	0.124	1.97	0.020
Isoform 2 of Glial fibrillary acidic protein	P14136-2	5.23	46	1.02	0.856	1.63	0.017	1.66	0.033
Isoform 2 of Glial fibrillary acidic protein	P14136-2	5.09	36	-2.19	0.036	2.42	0.027	1.10	0.639
Isoform 2 of Glial fibrillary acidic protein	P14136-2	5.74	48	2.04	0.041	-1.60	0.157	1.27	0.292
Isoform 2 of Glial fibrillary acidic protein	P14136-2	5.16	49	-1.19	0.337	1.53	0.040	1.28	0.139
Isoform 2 of Glial fibrillary acidic protein	P14136-2	5.07	37	-1.53	0.009	1.56	0.006	1.02	0.726
Isoform 2 of Glial fibrillary acidic protein	P14136-2	5.5	46	-1.08	0.550	1.60	0.047	1.48	0.029
Isoform 2 of Glial fibrillary acidic protein	P14136-2	5.17	38	-1.12	0.100	1.63	0.016	1.46	0.045
Isoform 2 of Glial fibrillary acidic protein	P14136-2	5.16	35	-1.91	0.002	1.70	0.002	-1.12	0.175
Isoform 3 of Dynamin-1	Q05193-3	4.88	19	-1.35	0.015	-1.60	0.016	-2.16	0.001
Isoform 3 of Dynamin-1	Q05193-3	4.93	20	-1.23	0.257	1.69	0.016	1.38	0.094
Isoform 3 of Peroxiredoxin-5, mitochondrial	P30044-3	7.7	15	1.29	0.081	-1.77	0.009	-1.37	0.005
Isoform 3 of Ras-related protein Rap-1b	P61224-3	6.37	19	-1.19	0.034	1.92	0.006	1.62	0.015
Isoform CNPI of 2',3'-cyclic-nucleotide 3'-phosphodiesterase	P09543-2	9.11	40	-1.66	0.127	1.82	0.293	1.10	0.970
Isoform Cytoplasmic+peroxisomal of Peroxiredoxin-5, mitochondrial	P30044-2	7.75	16	1.31	0.335	-2.27	0.088	-1.73	0.123
Isoform IB of Synapsin-1	P17600-2	8.87	74	1.17	0.376	-2.00	0.032	-1.71	0.056
Isoform IB of Synapsin-1	P17600-2	9.17	75	1.16	0.173	-1.72	0.001	-1.48	0.005
Isoform Non-brain of Clathrin light chain A	P09496-2	4.69	30	-1.01	0.933	-3.31	0.005	-3.34	0.004
Keratin, type I cytoskeletal 10	P13645	5.33	102	-1.04	0.794	-1.80	0.019	-1.87	0.018
Keratin, type I cytoskeletal 9	P35527	4.82	13	-1.21	0.405	-1.56	0.179	-1.89	0.046
Keratin, type I cytoskeletal 9	P35527	6.14	17	-1.37	0.076	1.55	0.072	1.13	0.469
Keratin, type II cytoskeletal 1	P04264	5.54	17	1.33	0.811	-3.10	0.370	-2.33	0.022

Protein name	Accession No.	pI	MW (kD)	AD vs. control	p - Value	NDAN vs. AD	p - Value	NDAN vs. control	p - Value
Keratin, type II cytoskeletal 1	P04264	4.66	35	-1.14	0.118	-1.81	0.001	-2.07	0.000
Keratin, type II cytoskeletal 1	P04264	7.55	12	1.32	0.067	-1.54	0.105	-1.17	0.447
Malate dehydrogenase, mitochondrial	P40926	8.94	30	1.67	0.005	1.77	0.102	2.97	0.016
NADH dehydrogenase [ubiquinone] 1 alpha subcomplex subunit 5	F8WAS3	5.5	13	-3.21	0.134	-1.44	0.869	-4.62	0.040
NADH dehydrogenase [ubiquinone] flavoprotein 1, mitochondrial (Fragment)	E9PQP1	8.26	46	2.77	0.003	-1.47	0.208	1.88	0.195
Neurofilament medium polypeptide	E7EMV2	5.4	50	-1.28	0.321	1.50	0.241	1.17	0.635
Profilin-2	C9J0J7	5.06	13	1.01	0.929	-2.08	0.047	-2.06	0.026
Profilin-2	C9J0J7	5.76	14	1.80	0.523	-1.54	0.684	1.17	0.554
Pyruvate carboxylase, mitochondrial	P11498	6.28	119	1.12	0.577	-1.59	0.048	-1.42	0.042
Rho GDP-dissociation inhibitor 1 (Fragment)	J3KTF8	5.02	20	1.18	0.094	-1.77	0.009	-1.50	0.033
Septin-7	F5GZE5	8.68	45	1.48	0.336	-1.66	0.075	-1.12	0.908
Spectrin alpha chain, non-erythrocytic 1	Q13813	5.38	134	1.22	0.465	-1.91	0.039	-1.56	0.202
Syntaxin-binding protein 1	P61764	5.52	31	1.12	0.359	2.00	0.001	2.24	0.001
Tubulin alpha-1A chain (Fragment)	F8VRZ4	5.09	22	-2.13	0.032	1.56	0.233	-1.37	0.299
Tubulin alpha-1B chain (Fragment)	F8VVB9	5.23	33	-1.32	0.050	-2.97	0.041	-3.93	0.021
Tubulin alpha-1B chain (Fragment)	F8VVB9	5.29	33	-1.26	0.377	-1.66	0.110	-2.09	0.020
Tubulin alpha-1B chain (Fragment)	F8VVB9	5.54	46	-1.31	0.006	2.04	0.004	1.55	0.021
Tubulin beta-2A chain	Q13885	5.45	34	1.19	0.490	-1.84	0.184	-1.55	0.421
Tubulin beta-4A chain	P04350	4.81	16	-1.20	0.137	-1.84	0.004	-2.20	0.001
Tubulin beta-6 chain (Fragment)	K7ESM5	5.26	12	-1.59	0.298	-2.51	0.098	-4.01	0.036
Ubiquitin carboxyl-terminal hydrolase isozyme L1	D6R974	5.15	20	1.04	0.877	-2.47	0.022	-2.37	0.019

Supplementary table 1. Postsynaptic density proteins identified using MS/MS that are included in the discussion.